University Library

MINERVA ACCESS

A gateway to Melbourne's research publications

Minerva Access is the Institutional Repository of The University of Melbourne

Author/s:
Ngo, HB;Melo, MR;Layfield, S;Connelly, AA;Bassi, JK;Xie, L;Menuet, C;McDougall, SJ;Bathgate, RAD;Allen, AM

Title:
A Chemogenetic Tool that Enables Functional Neural Circuit Analysis

Date:
2020-09-15

Citation:
Ngo, H. B., Melo, M. R., Layfield, S., Connelly, A. A., Bassi, J. K., Xie, L., Menuet, C., McDougall, S. J., Bathgate, R. A. D. & Allen, A. M. (2020). A Chemogenetic Tool that Enables Functional Neural Circuit Analysis. CELL REPORTS, 32 (11), https://doi.org/10.1016/j.celrep.2020.108139.

Persistent Link:
https://hdl.handle.net/11343/252570

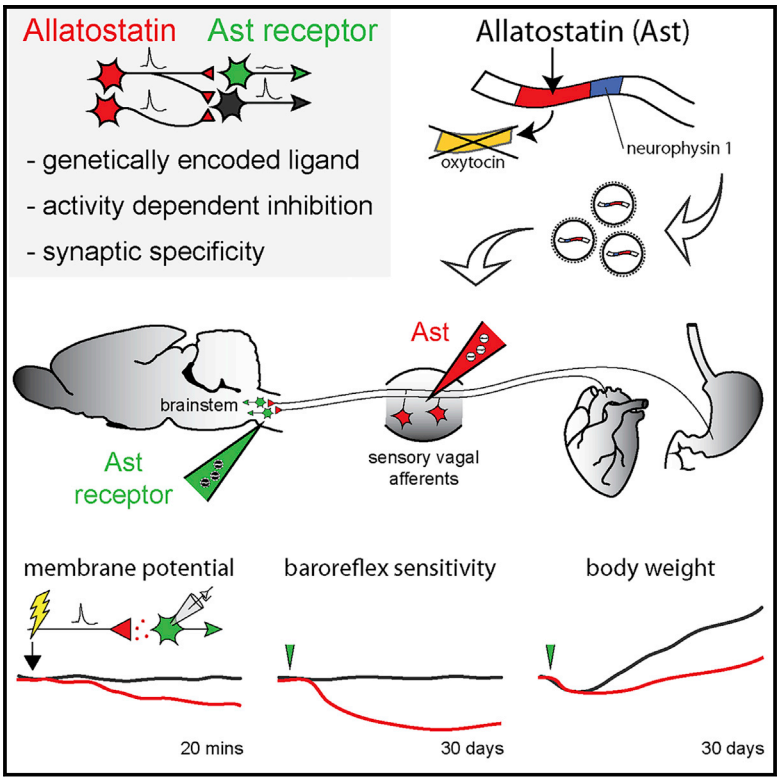
License:
CC BY-NC-ND

Cell Reports

Resource

A Chemogenetic Tool that Enables Functional Neural Circuit Analysis

Graphical Abstract



Authors

Hoai Buu Ngo, Mariana R. Melo, Sharon Layfield, ..., Stuart J. McDougall, Ross A.D. Bathgate, Andrew M. Allen

Correspondence

a.allen@unimelb.edu.au

In Brief

Chemogenetics provides understanding of the function of specific neurons transduced to express an actuating receptor that is affected by global ligand administration. Ngo et al. generate a viral vector that induces neuronal expression and synaptic release of the inhibitory chemogenetic ligand, allatostatin, enabling circuit-based inhibition of allatostatin receptor-expressing neurons.

Highlights

- Oxytocin is replaced in its precursor with the insect peptide allatostatin (Ast)
- Viral expression induces activity-dependent, synaptic release of bioactive Ast
- Ast is expressed in vagal afferents and Ast receptor in Phox2 NTS neurons
- This induces a long-term reduction in baroreceptor sensitivity and bodyweight gain

Ngo et al., 2020, Cell Reports *32*, 108139
September 15, 2020 © 2020 The Author(s).
https://doi.org/10.1016/j.celrep.2020.108139

CellPress

Cell Reports

CellPress
OPEN ACCESS

Resource

A Chemogenetic Tool that Enables Functional Neural Circuit Analysis

Hoai Buu Ngo,[1] Mariana R. Melo,[2] Sharon Layfield,[1] Angela A. Connelly,[2] Jaspreet K. Bassi,[2] Lin Xie,[2] Clément Menuet,[2,3] Stuart J. McDougall,[1] Ross A.D. Bathgate,[1,4,5] and Andrew M. Allen[1,2,5,6,*]

[1]Florey Institute of Neuroscience and Mental Health, University of Melbourne, Parkville, VIC 3010, Australia
[2]Department of Physiology, University of Melbourne, Parkville, VIC 3010, Australia
[3]Institut de Neurobiologie de la Méditeranée, INMED UMR1249, Aix-Marseille Université, Marseille, France
[4]Department of Biochemistry and Molecular Biology, University of Melbourne, Parkville, VIC 3010, Australia
[5]Senior author
[6]Lead Contact
*Correspondence: a.allen@unimelb.edu.au
https://doi.org/10.1016/j.celrep.2020.108139

SUMMARY

Chemogenetics enables manipulation of neuronal activity in experimental animals. While providing information about the transduced neuron expressing a ligand-activated molecule, chemogenetics does not provide understanding about the antecedent circuit that drives that neuron's activity. For current approaches, this is not feasible, because the activating molecules are not genetically encoded. The insect allatostatin/allatostatin receptor system, a highly specific, powerful inhibitory chemogenetic approach, has this advantage, because the ligand, being a peptide, is genetically encoded. We developed viral vector-based systems to express biologically active allatostatin in neurons *in vivo* and allatostatin receptors in subpopulations of postsynaptic neurons. We demonstrate that activity-dependent release of allatostatin induces inhibition of allatostatin receptor-expressing neurons. We validate the approach in the vagal viscerosensory system where inhibitory, rather than the usual excitatory, viscerosensory input leads to sustained decreases in baroreceptor reflex sensitivity and bodyweight.

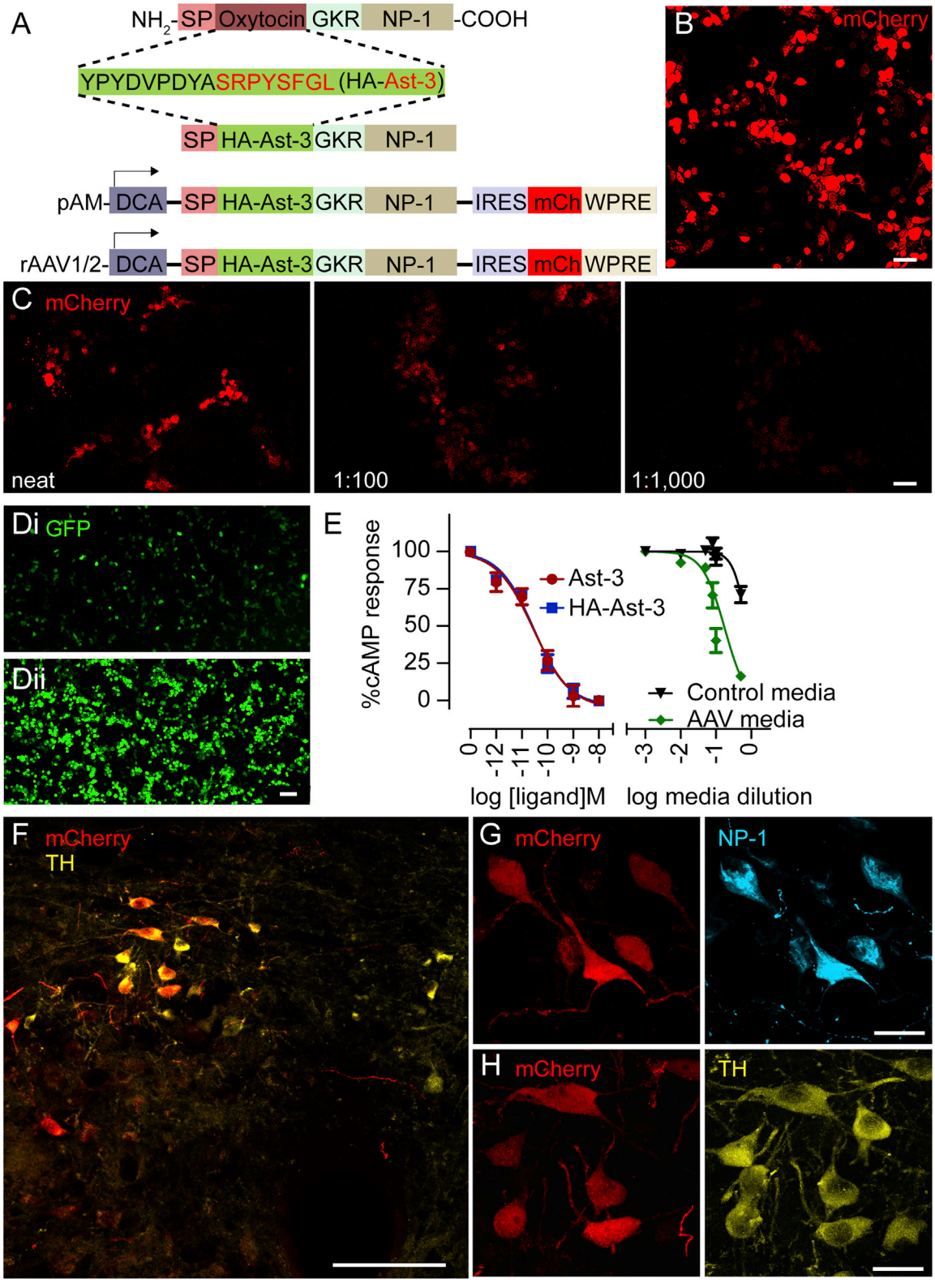
INTRODUCTION

Optogenetic and chemogenetic methods have advanced understanding of the role of specific neurons in behaviors (Deisseroth, 2015; Roth, 2016). A chemogenetic approach that provides specific and powerful inhibition of neuronal activity is the insect allatostatin (Ast) system (Tan et al., 2006). The Ast receptor (AstR) is related to several mammalian receptors, including the somatostatin receptor, and links via $G_{i/o}$ G proteins to inhibit cyclic adenosine monophosphate (cAMP) and activate G-protein-coupled inward-rectifier potassium (GIRK) channels (Birgül et al., 1999). The AstR is not activated by any known mammalian ligands, and its expression alone does not alter cell activity (Birgül et al., 1999; Lechner et al., 2002; Menuet et al., 2017). Similarly, Ast is inert within the mammalian nervous system (Birgül et al., 1999; Menuet et al., 2017), thus overcoming some issues around other chemogenetic approaches (Gomez et al., 2017). Adoption of the Ast system for mammalian neuroscience studies has been impeded by the need to deliver the peptide ligand directly into the brain. However, this also represents an advantage because, unlike the activator for other chemogenetic and optogenetic approaches, Ast is genetically encoded, enabling transgenic expression. We predicted this expression would lead to activity-dependent release of the chemogenetic ligand to affect only postsynaptic neurons transduced to express the receptor—a circuit- and activity-based chemogenetic approach. This provision of the activating chemogenetic ligand by the antecedent cell is impossible for optogenetics and not available for any other chemogenetic system.

We generated a construct based upon the oxytocin precursor to enable expression of Ast by neurons *in vivo*, in combination with an essential amidating sequence and trafficking molecule. We validated this method using the vagal viscerosensory system—transducing vagal afferent neurons, which normally excite their postsynaptic neuron, to express Ast such that their activity would hyperpolarize AstR-expressing neurons in the brainstem nucleus of the solitary tract (NTS). Studying vagal afferents has the advantage of anatomical separation between the somata of the visceral afferents in the nodose ganglion (NDG) that were transduced to express Ast and those of the NTS neurons that were transduced to express the AstR. Issues such as transduction of axons of passage or spread of viral injectate were thus eliminated.

Vagal viscerosensory afferent neurons are pseudounipolar neurons with their somata located in the NDG and peripheral axons that terminate widely throughout the viscera. Vagal mechanoreceptor terminals in the aortic arch and heart provide information that contributes to cardiovascular reflexes, including the baroreceptor reflex (Osborn and England, 1990), while mechano- and chemoreceptor afferents in the gastrointestinal tract

This is an open access article under the CC BY-NC-ND license (http://creativecommons.org/licenses/by-nc-nd/4.0/).



(legend on next page)

provide information about the amount and composition of ingested food and thus contribute to nutrition and bodyweight homeostasis (Williams et al., 2016). The central axons of vagal viscerosensory afferents project to the NTS, where they provide strong glutamatergic input to second-order neurons (Andresen et al., 2001). The NTS has a heterogeneous population of neurons with different neurochemical phenotypes, with one prominent class expressing the transcription factors Phox2a or Phox2b (Card et al., 2010; Dauger et al., 2003; Stornetta et al., 2006). For this study, we have utilized a lentivirus (Lv), with selectivity for Phox2-expressing neurons, to transduce caudal NTS (cNTS) neurons with the AstR. Because the physiology of this system is relatively well characterized, we reasoned that inhibition would provide predictable outcomes. In addition, targeting vagal afferents was predicted to provide valuable information that is not attainable with surgical approaches, as animals do not recover from bilateral cervical vagotomy. Using this enhanced chemogenetic approach in rats, we demonstrate that inhibition of ongoing vagal afferent input to Phox2-expressing cNTS neurons impairs baroreceptor reflex function, associated with an increase in blood pressure (BP), and alters bodyweight homeostasis. Together, the data validate a chemogenetic approach that enables interrogation of active neural circuits *in vivo*.

RESULTS

Generation of an Allatostatin-Expressing Construct

The Ast precursor contains sequences of multiple other peptides, thus ruling out direct cloning to achieve Ast expression in mammalian cells. We also needed to ensure correct amidation of transgenic Ast to retain bioactivity (Bendena et al., 1997) and trafficking to enable vesicular release from neurons. The precursor for oxytocin, which includes a signal peptide, C-terminal amidating motif, and neurophysin I (NP-1) (Ivell and Richter, 1984) that facilitates processing and trafficking, was used as a neuropeptide precursor backbone for incorporating the Ast sequence (Figure 1A). We excised the *Drosophila melanogaster* Ast-3 sequence, which has been used in other chemogenetics studies (Lechner et al., 2002), and added a hemagglutinin (HA) epitope tag to the amino terminal, because there are no specific Ast antibodies available, to generate HA-Ast-3. The oxytocin sequence was excised from its precursor and HA-Ast-3 inserted between the signal peptide and the amidation motif. We incorporated the fluorophore mCherry downstream of an internal ribosome entry site (IRES), providing the final plasmid designed to express HA-Ast-3, NP-1, and mCherry under the control of a CMV-chicken β-actin hybrid (DCA) promoter (Figure 1A). This construct is abbreviated to HA-Ast-3-mCherry. This precursor sequence (Figure S1A) was cloned into an adeno-associated virus (AAV) plasmid (pAM- HA-Ast-3-mCherry; Figure S1B) and used to make the recombinant AAV rAAV1/2-HA-Ast-3-mCherry with a titer, determined by qPCR, of 5.08×10^{11} genome copies/mL.

Transgenic Allatostatin Is Biologically Active *In Vitro*

Transfection of HEK293T cells with pAM-HA-Ast-3-mCherry (Figure 1B) or transduction with dilutions of rAAV1/2-HA-Ast-3-mCherry (Figure 1C) resulted in robust expression of mCherry, even at 1:1,000 viral dilution, verifying the functionality of the construct and the purified AAV. To test the activity of Ast-3 peptides, we developed stably transduced AstR-expressing CHO-K1 cells using Lv transduction (Lv-CBA-AstR-IRES-GFP) followed by fluorescence-activated cell sorting (FACS) (Figure 1D). We used these cells in a robust assay for measurement of cellular cAMP activity (Bathgate et al., 2006). Because the AstR couples via $G_{\alpha i}$ to inhibit cAMP production, the cells were first stimulated by the adenylate cyclase activator forskolin and then exposed to different concentrations of synthetic Ast-3 and HA-Ast-3 or to dilutions of conditioned media from a separate population of HEK293T cells transfected for 48 h with pAM-HA-Ast-3-mCherry or pcDNA3.1, a control empty plasmid (Figure 1E). Both Ast-3 and HA-Ast-3 showed equivalent potency to inhibit cAMP (pEC_{50} 10.47 ± 0.27 and 10.61 ± 0.08 nM, respectively; n = 4 assays), indicating that the HA-tag did not affect the activity of the peptide. Serial dilutions of conditioned media from pAM-HA-Ast-3-mCherry transfected cells also inhibited cAMP levels with maximal inhibition at 1:5 dilution, indicating production and release of biologically active HA-Ast-3. Conditioned media from control cells had only a minor effect at 1:5 dilution. Comparison with the effect of synthetic peptide suggests an HA-Ast-3 concentration in the conditioned media of ~1 nM.

Viral Transduction Leads to Transgene Expression and Trafficking in Neurons *In Vivo*

To examine transgene expression and cellular tropism, we anesthetized animals and microinjected rAAV1/2-HA-Ast-3-mCherry

Figure 1. Generation and Validation of an Allatostatin-Expressing Viral Construct

(A) Schematic diagram outlining the oxytocin precursor backbone, the insertion of hemagglutinin-tagged (HA) allatostatin (Ast-3), and generation of expression plasmids

(B–D) Expression of transgenes, as evidenced by the fluorophore mCherry was tested by plasmid transfection (B) or incubation with recombinant adeno-associated virus (rAAV1/2-HA-Ast-3-mCherry) at different dilutions (C) in HEK293T cells. Stably transfected Ast receptor (AstR)-expressing CHO-K1 cells were generated by incubation with Lv-CBA-AstR-IRES-GFP (Di) and showed more robust expression after FACS based on GFP expression (Dii).

(E) Both synthetic Ast-3 and HA-Ast-3, as well as conditioned media from HEK293T cells transfected with the pAM-HA-Ast-3-mCherry (AV media), induced dose-dependent inhibition of cAMP from forskolin-stimulated, stably transduced AstR-expressing CHO-K1 cells. Media from empty control plasmid pcDNA3.1(+)-transfected cells (control media) only affect cAMP levels when undiluted. Data are mean ± SEM (n = 4 assays with triplicate measures within each assay).

(F–H) Injection of rAAV1/2-HA-Ast-3-mCherry into the dorsomedial medulla of the rat induced neuronal expression of mCherry (red) in the vicinity of the injection site (F), including in tyrosine hydroxylase-immunoreactive (TH; yellow) NTS neurons. Co-expression of mCherry and neurophysin-1 (NP-1; blue; G) and mCherry and TH (H) is shown in higher power. The scale bars depict 100 μm with the exception of (G) and (H) where they represent 20 μm. The scale bar in (B) applies to (C).

Abbreviations: DCA, hybrid cytomegalovirus enhancer/chicken β-actin promoter; GKR, amidation motif; IRES, internal ribosome entry site; mCh, mCherry fluorophore; NP 1, neurophysin 1; SP, signal peptide; WPRE, woodchuck posttranscriptional regulatory element.

Table 1. Coordinates Used for Injections into the Caudal Nucleus of the Solitary Tract in Animals Used for Patch-Clamp Electrophysiology Studies

Injection Number	Rostro-Caudal Plane (mm)	Medio-Lateral Plane (mm)
1, 2	−0.4	0
3, 4	−0.25	0
5, 6	−0.1	0
7–10	+0.1	± 0.1
11–14	+0.25	± 0.2
15–18	+0.4	± 0.3

Measurements in the rostro-caudal plane are in relation to obex. 50 nL of Lv-PRSx8-AstR or Lv-PRSx8-GFP was injected slowly at each site to give a total injection volume of 900 nL.

Table 2. Coordinates Used for Injections into the Caudal Nucleus of the Solitary Tract in Animals Used for Blood Pressure and Bodyweight Studies

Injection Number	Rostro-Caudal Plane (mm)	Medio-Lateral Plane (mm)
1	−0.4	0
2	−0.25	0
3	−0.1	0
4, 5	+0.1	± 0.1
6, 7	+0.4	± 0.3

Measurements in the rostro-caudal plane are in relation to obex. 50 nL of Lv-PRSx8-AstR or Lv-PRSx8-GFP was injected slowly at each site to give a total injection volume of 350 nL.

(Tables 1 and 2) into the dorsomedial medulla. Immunohistochemistry was performed 4 weeks after injection, and co-expression of mCherry and NP-1 was observed in neurons expressing the catecholamine-synthesizing enzyme tyrosine hydroxylase (TH) in the NTS (Figures 1F–1H) or those expressing choline acetyl transferase (ChAT; not shown) in the dorsal motor nucleus of vagus (DMV).

Microinjection of rAAV1/2-HA-Ast-3-mCherry bilaterally into the NDG (Figure 2A) resulted in robust expression of HA-tag, mCherry, and NP-1 in the somata of NDG neurons (Figure 2B) and their central projections in the NTS (Figures 2C–2L). Immunohistochemical detection of the HA-tag proved unreliable *in vivo*, particularly in axonal projections. Because NP-1 is produced and secreted alongside the fully mature peptide (Rao et al., 1992), we concentrated on NP-1 and mCherry for further validation of transgene expression. Axon fascicles expressing mCherry were observed coursing from the dorsolateral surface of the brainstem into the solitary tract (ST) (Figure 2C) and then projecting into the NTS throughout its rostro-caudal extent (Figures 2C–2E). The projections within the NTS increased in density at more caudal levels. The axons in the NTS expressed mCherry and NP-1 (Figure 2F), which clearly distinguished them from the axons of oxytocinergic parvocellular hypothalamic neurons that project to this region but only express NP-1 (Figure 2F). At mid-levels of the NTS (Figure 2D), we observed a small number of mCherry axons in the paratrigeminal nucleus (Figure 2G). This labeling was sparse, indicating that the majority of transduction from our injection protocol occurred in the NDG, with little in the adjacent jugular ganglion. Also, at this mid-NTS level, mCherry expression was clearly observed in close proximity to TH neurons in the area postrema (AP) (Figure 2H). We also observed viscerosensory afferents closely apposed to cholinergic motor neurons in the DMV (Figures 2I and 2J). Within the NTS, many dendrites of TH-expressing A2 neurons showed close appositions with transduced viscerosensory afferents (Figure 2K).

Ast-Expressing Viscerosensory Neurons Projecting to AstR-Expressing NTS Neurons

Following microinjection of rAAV1/2-HA-Ast-3-mCherry into the NDG bilaterally and Lv-PRSx8-AstR-GFP into the cNTS, we observed overlapping expression of GFP and mCherry in the NTS (Figure 3). Expression of GFP was observed throughout the cNTS, predominantly in the medial subnuclei (Figures 3A–3C). We observed co-localization of GFP with NTS TH-expressing neurons as well as substantial numbers of non-TH-expressing neurons (Figure 3F). The GFP expression also occurred in ChAT-expressing DMV neurons ventral to the NTS (Figure 3E), while the dorsally located AP was relatively devoid of AstR expression (Figure 3A). In all animals, we observed overlapping expression of mCherry-, GFP-, and TH-expressing neurons in the NTS (Figure 3G). We also observed mCherry-expressing vagal afferent axons making numerous close appositions with AstR-expressing NTS neurons (Figures 3G and 3H).

Transduced Viscerosensory Afferents Show Activity-Dependent Release of Active Allatostatin

To determine whether electrical stimulation of viscerosensory axons would induce release of Ast-3 and influence the activity of AstR-expressing NTS neurons, we microinjected rAAV1/2-HA-Ast-3-mCherry into the NDG and either Lv-PRSx8-AstR-GFP or Lv-PRSx8-GFP into the NTS. After 6 weeks, we prepared horizontal slices of the medulla oblongata that enabled visualization of both the ST and the NTS. Whole-cell patch-clamp recordings were made of GFP-expressing neurons from experimental and control animals. Superfusion with synthetic HA-Ast-3 (100 nM) or Ast-3 (5 nM) resulted in sustained hyperpolarization (~10 mV) of AstR-expressing neurons but no alteration in membrane potential in GFP-only transduced or non-transduced cells (Figures 3I and 3J). High-frequency electrical stimulation of the ST (50 Hz for 30 s) to activate viscerosensory afferents in the presence of a cocktail of antagonists to inhibit ionotropic receptors resulted in a slowly developing, sustained hyperpolarization (~5–10 mV) in AstR-expressing neurons that peaked at 388 ± 57 s. This stimulation did not alter the membrane potential in control cells (Figures 3I and 3J). In two of these neurons, application of the voltage-gated sodium channel blocker tetrodotoxin (TTX) to block action-potential-dependent transmitter release (Figures 3I and 3J) prevented the change in membrane potential induced by ST stimulation. A step current injection protocol was used to induce action potential firing in AstR-expressing neurons (Figures 3K–3M). When combined with high-frequency electrical stimulation of the ST, the number of current-induced action potentials was substantially reduced. Together, these anatomical

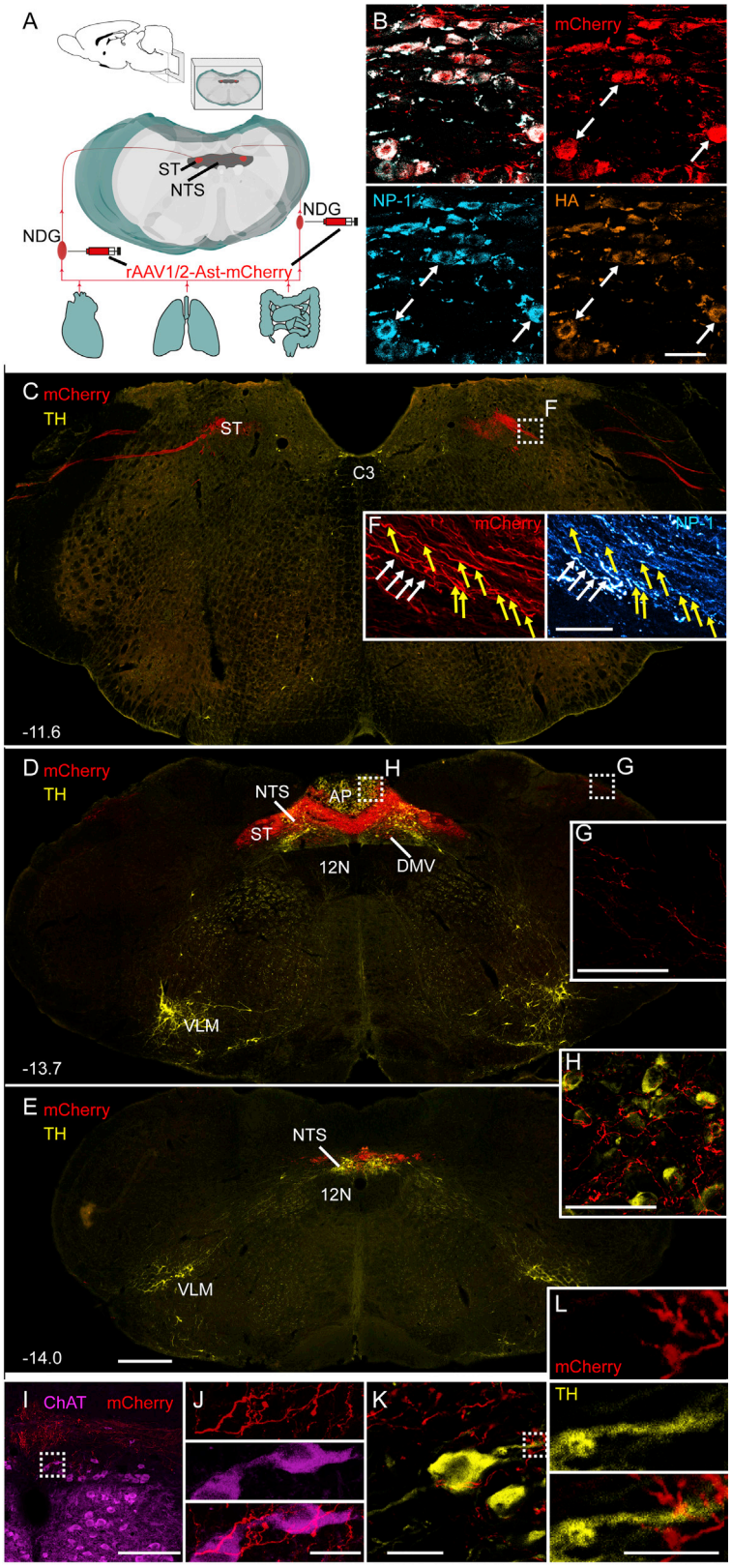


Figure 2. Expression of Allatostatin in Vagal Viscerosensory Neurons and Their Terminal in the Nucleus of the Solitary Tract following Viral Microinjection in the Nodose Ganglion

(A) The schematic diagram outlines the experimental paradigm. The position of the brain region studied is shown in the sagittal plane and, in the box, in the coronal plane. The enlarged model shows the position of the nucleus of the solitary tract (NTS) in the medulla oblongata as well as the solitary tract (ST). The somata of vagal viscerosensory neurons are located in the nodose ganglion (NDG). Their peripheral axons sense different stimuli in the viscera, and the central axons project via the ST to synapse on NTS neurons. rAAV1/2-HA-Ast-3-mCherry was injected bilaterally into the NDG.

(B) Following microinjection of rAAV1/2-Ast-3-mCherry into the NDG, transgene expression was detected in sections of the NDG using immunohistochemistry to visualize mCherry, neurophysin-1 (NP-1), and HA-tag. The overlay of each color channel is shown in the top-left panel. The arrows highlight neurons that express all transgenes. Expression of mCherry in the central axons of transduced NDG neurons was examined in coronal sections through the rostro-caudal extent of the rat brainstem, along with immunohistochemistry for tyrosine hydroxylase (TH; C–E; rostro-caudal levels indicated relative to Bregma [mm]).

(C and F) At the most rostral level, indicated by TH labeling in dorsomedial C3 neurons, mCherry-expressing axons are observed traversing the medulla from the dorsolateral entry point of the vagal afferent trunks to the medial solitary tract (C). Higher-power magnification of ST axons show that they express mCherry and NP-1 (F; yellow arrows). The white arrows highlight a NP-1 axon that does not express mCherry and is likely to arise from an endogenous oxytocin-expressing neuron.

(D, E, and G–L) At mid-NTS, at the level of the area postrema (AP), dense mCherry-expressing fiber bundles are observed in the ST as well as throughout the NTS bilaterally (D). The dashed boxes outline areas of mCherry-expressing fibers that are shown in higher power in the insets (G and H). The parameters for capture of the higher-power images is matched, showing that only sparse, low-level expression of mCherry afferents is observed in the paratrigeminal nucleus (Pa5; G), indicating little transduction of jugular ganglion neurons. The vagal afferent input to the AP makes close appositions with TH-expressing AP neurons (H). At the most caudal level (E), the mCherry labeling is less dense but remains extensive throughout the caudal NTS. mCherry-expressing axons are also observed in the region of the dorsal motor nucleus of vagus, in close proximity to choline acetyl transferase (ChAT) neurons (I) located dorsal to the motor neurons of the hypoglossal nucleus. A single focal plane confocal image (1 μm thickness) of the boxed area is shown at higher magnification (J), showing close appositions between mCherry-expressing vagal afferents and ChAT-expressing parasympathetic preganglionic neurons in the dorsal motor nucleus of the vagus. Individual color channels and the merged image. Within the NTS, mCherry-expressing afferents are observed in close proximity to TH-expressing A2 NTS neurons (K), forming close appositions with A2 neuron dendrites. A single focal plane (1 μm thickness) confocal image of the boxed area is shown at higher magnification, with the colors separated to highlight close appositions (L). The scale bar in (B) depicts 50 μm; (C)–(E) 500 μm; (F) 20 μm; (G) and (H) 50 μm; (I) 200 μm; (J) and (K) 20 μm; (K) insets 10 μm. Abbreviations: 12N, hypoglossal nucleus; ST, solitary tract; AP, area postrema; C3, C3 adrenergic cell group; DMV, dorsal motor nucleus of vagus; NTS, nucleus of the solitary tract; VLM, ventrolateral medulla.

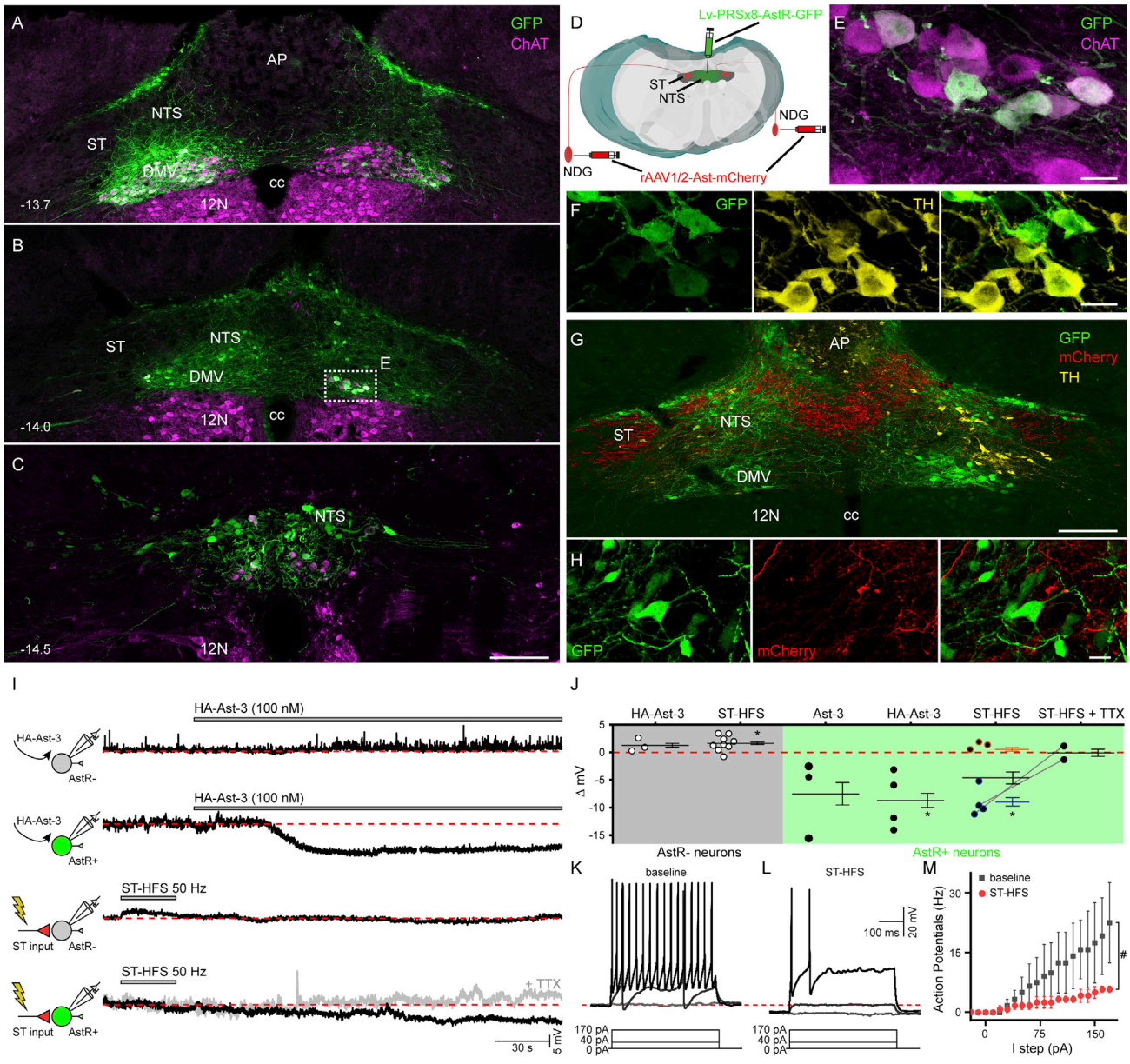


Figure 3. Anatomical and Electrophysiological Examination of the Interaction between Allatostatin-Expressing Viscerosensory Afferents and Allatostatin Receptor-Expressing Nucleus of the Solitary Tract Neurons

(A–C) Three representative coronal sections of the medulla from one animal, organized from rostral (A) to caudal (C) with levels relative to bregma (mm), are shown. Expression of GFP is observed in the nucleus of the solitary tract (NTS), and the dorsal motor nucleus of vagus (DMV) following microinjection of Lv-PRSx8-AstR-GFP. Immunoreactivity for choline acetyltransferase (ChAT) is also shown, indicating the distribution of DMV and hypoglossal motor neurons.

(D) A schematic diagram showing the injections made in this protocol, which applies to all subsequent experimental animals, is shown. rAAV1/2-HA-Ast-3-mCherry was first injected bilaterally into the nodose ganglia (NDG), and 2–4 weeks later Lv-PRSx8-AstR or Lv-PRSx8-GFP was injected into the caudal NTS.

(E) A higher-power, single focal plane (1 μm thickness) confocal image of the boxed area in (B) showing co-localization between GFP- and ChAT-expressing parasympathetic preganglionic neurons in the DMV.

(F) Co-localization of GFP and tyrosine hydroxylase (TH) A2 neurons in the NTS is shown.

(G) In experimental animals that received microinjections of rAAV1/2-HA-Ast-3-mCherry into the nodose ganglion, substantial overlap in the distribution of mCherry-expressing vagal afferent neurons, AstR-GFP-expressing neurons, and TH-expressing neurons is observed.

(H) Close appositions between GFP-expressing neurons and mCherry-expressing vagal afferent terminals in the NTS were commonly observed, as shown in this maximum projection, confocal image.

(I) Whole-cell recordings were taken from both AstR-GFP- and non-AstR-expressing neurons in the NTS from rats expressing HA-Ast-3-mCherry in vagal afferents. Individual neurons are shown with the schematic indicating Lv-PRSx8-AstR (AstR$^+$, green) and Lv-PRSx8-GFP (AstR$^-$, gray) transduced neurons.

(legend continued on next page)

and functional studies provide confidence that the rAAV1/2-HA-Ast-3-mCherry transduction of NDG neurons results in the expression of Ast-3 that is transported to the terminals of viscerosensory neurons in the NTS and released from synapses in response to action potentials. When released, the Ast-3 hyperpolarizes postsynaptic AstR-expressing neurons.

Transgenic Allatostatin Interacts with Postsynaptic Allatostatin Receptors to Modulate Blood Pressure *In Vivo*

Mechanosensitive vagal afferents send information from the heart and aorta to the NTS, with the high-pressure afferents from the aortic arch being a major contributor to the baroreceptor reflex (Osborn and England, 1990). Lesions of aortic arch baroreceptor afferents increase BP lability and temporarily increase BP (Osborn and England, 1990). Similarly, lesions of the A2 TH-expressing neuron group in the NTS, a subpopulation of Phox2-expressing NTS neurons, increase BP lability (Talman et al., 2012). We reasoned that inhibition of the Phox2-expressing neurons in the NTS by ongoing release of Ast-3 from the viscerosensory input should have a similar phenotype.

For this study, we utilized spontaneously hypertensive rats (SHR), a well-characterized model of neurogenic cardiovascular disease. In staged surgeries, with 2 weeks between each surgery, each rat received: (1) bilateral microinjections of rAAV1/2-HA-Ast-3-mCherry into the NDG; (2) implantation of BP telemeters into the abdominal aorta; and (3) microinjection of Lv-PRSx8-AstR-GFP (SHR experimental) or Lv-PRSx8-GFP (SHR control) into the cNTS. Experiments conducted in the nine SHR experimental and eight SHR control are shown in Figure S2. However, as outlined in detail in the STAR Methods, three rats of each group were excluded from full analysis due to a sampling error during recordings. Both datasets show identical trends. Prior to NTS microinjections, SHR experimental and SHR control groups had similar cardiovascular function (Figures 4 and S2) (SHR experimental: systolic blood pressure [sBP]: 167 ± 4 mm Hg; diastolic blood pressure [dBP]: 114 ± 4 mm Hg; mean blood pressure [mBP]: 131 ± 3 mm Hg; heart rate [HR]: 282 ± 5 beats per minute [bpm]; SHR control: sBP: 161 ± 3 mm Hg; dBP: 118 ± 3 mm Hg; mBP: 132 ± 2 mm Hg; HR: 294 ± 14 bpm; Bonferroni multiple comparison test $p > 0.05$). Following NTS injections, BP decreased in both groups but stabilized within 3 days and, in SHR control, remained not different from baseline for the remainder of the recording period. In the SHR experimental group, sBP began to increase 5 days after the NTS surgery and was significantly elevated, compared to the SHR control group, between days 7 and 14 (Figure 4C; repeated-measures [RM] two-way ANOVA, $F[32,288] = 6.082$, $p < 0.0001$). In SHR experimental rats, sBP remained elevated compared to the pre-surgery values for the rest of the study period (SHR-AstR, pre-surgery: 160 ± 2 mm Hg; day 31: 172 ± 4 mm Hg; $p < 0.05$). Similar patterns were also observed in dBP and mBP (Figure S2; RM two-way ANOVA, $F[32,228] = 2.064$, $p < 0.001$). There was no difference in HR between groups over the recording period (Figure 4D). Comparison of the circadian variation in sBP between groups at days 9–11 revealed that sBP was elevated throughout the cycle in the SHR experimental group (Figure S2).

Baroreceptor denervation increases BP lability and reduces HR variability in humans (Robertson et al., 1993) and experimental animals (Zeng et al., 2018) due to disruption of this negative feedback pathway (Osborn and England, 1990). We derived the interbeat interval (IBI, a surrogate of R-R interval) from the blood pressure waveform and measured the standard deviation of both IBI and sBP across groups (Figures 4E and 4F). Compared to SHR control, the variance of sBP increased in the SHR experimental (RM two-way ANOVA; $F[1,9] = 65.79$, $p < 0.0001$; day 8: standard deviation of sBP: SHR experimental: 9 ± 0.6 mm Hg; SHR control: 5 ± 0.1 mm Hg; Bonferroni multiple comparisons test, $p < 0.0001$), while that of IBI decreased between days 8 and 16 (day 8: standard deviation of the IBI: SHR experimental: 0.043 ± 0.01 ms; SHR control: 0.075 ± 0.004 ms; Bonferroni multiple comparisons test, $p < 0.0001$). Using a sequence method (Figure S3A), we measured the sensitivity of the baroreceptor reflex derived from naturally occurring fluctuations in sBP and IBI (Figure 4G). For increases in BP, when baroreceptor afferent activity, and thus activity-dependent release of Ast-3, would be increasing, we observed a significant reduction of the baroreceptor reflex sensitivity (BRS) in the SHR experimental (Figure 4G) starting on day 3 and continuing for the entire recording period (Figure 4; RM two-way ANOVA, $F[32,288] = 9.588$, $p < 0.0001$; Bonferroni multiple comparisons test, days 5–31). Even at day 31, a clear attenuation of BRS was observed (SHR experimental: 2.5 ± 0.1 ms/mm Hg; SHR control: 2.9 ± 0.1 ms/mm Hg, Bonferroni multiple comparisons test, $p = 0.0014$). For decreases in sBP, where baroreceptor afferent activity would decrease, we observed a less pronounced effect on BRS, although some periods of significant difference occurred (Figure S3B). In a tonically active system, such as in baroreceptor afferents, where increased activity will result in greater release of Ast-3 and less activity will result in less Ast-3 release, a more pronounced difference in the arm of the baroreceptor reflex involving increased activity is expected.

(J–L) The group data are shown in (J), divided into $AstR^-$ (gray) and $AstR^+$ (green). Application of synthetic HA-Ast-3 hyperpolarized AstR-GFP-expressing ($AstR^+$) NTS neurons, without affecting non-AstR-expressing ($AstR^-$) neurons. In the presence of fast ionotropic receptor blockers (NBQX, 20 μM; AP-5, 100 μM; gabazine, 3 μM), high-frequency electrical stimulation (HFS; 50 Hz for 30 s) of the solitary tract (ST) did not alter the membrane potential of $AstR^-$ neurons but hyperpolarized $AstR^+$ neurons. ST-HFS-evoked hyperpolarization was blocked by TTX (1 μM; I). ST-HFS, in the presence of fast ionotropic receptor blockers (NBQX, AP-5, and gabazine), hyperpolarized 4 of 7 $AstR^+$ neurons (blue, mean ± SEM), but not another 3 $AstR^+$ neurons (red mean ± SEM; J). Current injections, in the presence of fast ionotropic receptor blockers, initiated action potentials in recorded $AstR^+$ neurons (n = 3; a representative example shown in K). ST-HFS hyperpolarized this $AstR^+$ neuron (L) to suppress action potential firing.

(M) The data for all three neurons are shown (baseline in squares; post ST-HFS in red circles). The asterisks in (J) denote $p < 0.05$; Student's paired t test. The # in (M) denotes $p < 0.05$; two-way ANOVA. The scale bars depict 200 μm (A–C, G); 20 μm (E, F, and H). Abbreviations: 12N, hypoglossal nucleus; ST, solitary tract; AP, area postrema; DMV, dorsal motor nucleus of vagus; NTS, nucleus of the solitary tract.

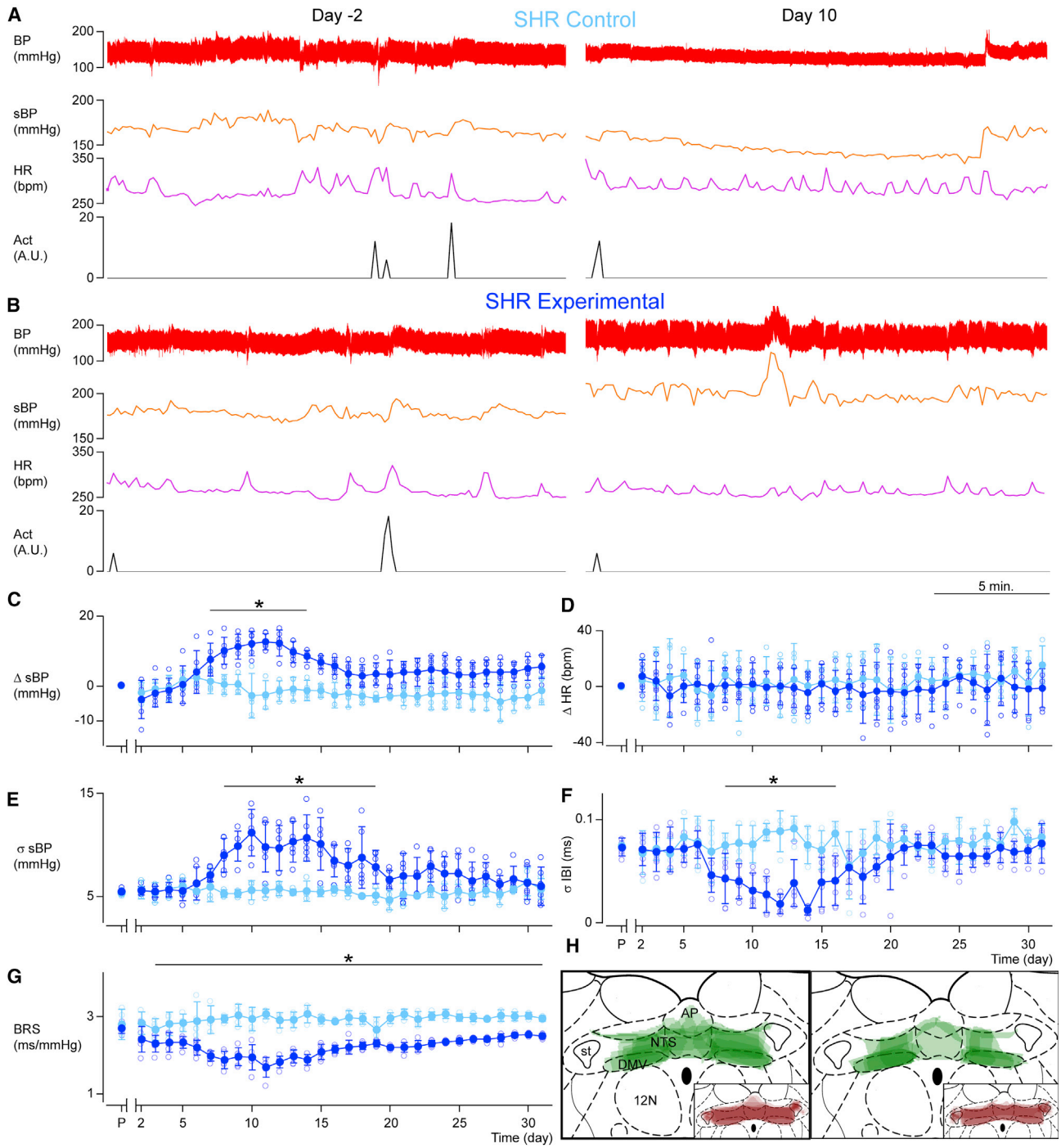


Figure 4. Cardiovascular Response to Inhibition of Vagal Afferent Input to Phox2-Expressing NTS Neurons

(A–G) Arterial pressure (BP, millimeters of mercury [mm Hg]), measured using in-dwelling blood pressure telemeters, was used to derive systolic blood pressure (sBP [mm Hg]) and heart rate (HR; beats per minute [bpm]; A). The telemeter also recorded animal movement in its home cage (Act [arbitrary units, a.u.]). The traces (A and B) show individual recordings during quiet light periods at 2 days prior to and 10 days after NTS injections in a control spontaneously hypertensive rat (SHR control) (A) and an SHR experimental (B) animal. Both groups received bilateral injections of rAAV1/2-HA-Ast-3-mCherry in the nodose ganglia 2 weeks prior to NTS injections. The SHR control (light blue) received Lv-PRSx8-GFP and the SHR experimental (dark blue) received Lv-PRSx8-AstR-GFP in the caudal NTS (C–G). The normalized group data are shown (n = 6 SHR experimental and n = 5 SHR control; mean ± 95% confidence interval [solid symbols]) in addition to individual values for each animal (open symbols). In each graph, the x axis shows time with p denoting an average of measurements derived over 3 days prior to surgery. The break in the x axis depicts the day of surgery. The graphs show the change (Δ) in sBP (C) and HR (D); the standard deviation (σ) of sBP (E) and of the

(legend continued on next page)

For all animals, the distribution of each transgene in the NTS was mapped (Figures 4H and S5). Immunohistochemical analysis revealed that all animals had extensive, bilateral transduction of viscerosensory afferent terminals in the NTS that overlapped with GFP expression within the cNTS as well as the DMV (Figures 2 and 3).

Transgenic Allatostatin Interacts with Postsynaptic Allatostatin Receptors to Modulate Bodyweight *In Vivo*

Vagal afferents convey chemoreceptor and mechanoreceptor information from the gastrointestinal tract and liver that plays an important role in bodyweight homeostasis. Although some of this information is important for signaling satiety, and hence its interruption might be expected in increased bodyweight (Williams et al., 2016), electrical vagal nerve block reduces bodyweight in obese subjects (Camilleri et al., 2008), as do lesions of the caudal NTS in rats (Hyde and Miselis, 1983).

The bodyweights of the SHR experimental and SHR control, included in the BP studies described above and including those removed from the BP analysis, were measured (Figure 5). At the start of the protocol, the SHR weighed 262 ± 7 g (~12 weeks of age), and there was no difference in bodyweight between rats assigned to each group (Student's unpaired t test, DF = 15, T = 1.387, p = 0.1858). In the immediate period following surgery, all rats had a decrease in bodyweight before recovering, and then exceeding, their pre-surgical weight (Figure 5). In the first two surgeries, for bilateral expression of Ast-3 in the NDG and implantation of BP telemeters, the two groups showed identical bodyweight changes (Figures 5A and S4; RM two-way ANOVA with Bonferroni multiple comparisons test; surgery 1: $F[1,15] = 0.9362$, $p = 0.3486$; surgery 2: $F[1,15] = 0.1587$, $p = 0.6726$; N.S.). Following injection of Lv into the NTS, SHR experimental and SHR control both showed immediate decreases in bodyweight, associated with the surgery, with a significant delay in return to control bodyweight in the SHR experimental group compared to the SHR control group (SHR control day 13 versus SHR experimental day 22). We observed a difference in bodyweight between the groups (RM two-way ANOVA $F[30,450] = 2.758$, $p < 0.0001$), with significant differences between days 4 and 30 (Bonferroni multiple comparisons test, $p < 0.05$).

To determine whether this was a phenotype associated with the SHR, we performed similar experiments in Sprague-Dawley (SD) rats without the BP telemeter implantation. At the start of the protocol, the SD rats weighed 236 ± 4 g (~8 weeks of age), and there was no difference in the bodyweights between the rats assigned to the two groups (Student's unpaired t test; DF = 20, T = 1.024, p = 0.3183). Analysis of bodyweights, divided post hoc into groups according to whether they received Lv-PRSx8-AstR-GFP (SD. experimental) or Lv-PRSx8-GFP (SD. control) microinjections into the cNTS, again revealed no difference in the bodyweight response to the first bilateral injections of rAAV1/2-HA-Ast-3-mCherry into the NDG (Figures 5B and S4). After the NTS injections, the bodyweights of both groups decreased, and like the SHR, there was a delay in return to baseline in the SD. experimental group (SD. control day 8 versus SD. experimental day 12). The bodyweights of the SD. experimental rats remained decreased compared to the SD. controls from day 12 until day 31 (RM two-way ANOVA $F[31,589] = 11.57$, $p < 0.0001$; Bonferroni multiple comparisons test, $p < 0.05$). At the completion of the study, there was a difference in bodyweight between groups (SD. experimental: 443 ± 5 g, SD. control: 476 ± 8 g; $p = 0.0156$). Post hoc immunohistochemical analysis confirmed extensive transduction of vagal afferents throughout the NTS that overlapped with Lv-transduced neurons in the cNTS and DMV (Figure S5).

In further control experiments, we observed no difference in the bodyweight response between SD. control and SD rats with unilateral, but not bilateral, transduction of Ast-3 in the NDG and Lv-PRSx8-AstR expression in the cNTS (Figure 5C, N.S.). Transduction of just the cNTS with either Lv-PRSx8-GFP or Lv-PRSx8-AstR also did not affect bodyweight homeostasis (Figure 5D). We conclude that ongoing vagal afferent stimulation of Phox2-expressing neurons in the cNTS is required for physiological maintenance of bodyweight.

DISCUSSION

Using the oxytocin precursor as a backbone, we have generated a plasmid for the production, processing, and trafficking of the insect peptide Ast-3 and validated the expression and release of Ast-3 in cells *in vitro* and in neurons *in vivo*. The Ast-3 released from transfected cells *in vitro* is bioactive at the AstR to inhibit cAMP production. Following transduction of NDG neurons, there is expression and trafficking of the transgenes to the central terminals of these viscerosensory afferent neurons in the NTS. The terminals make close appositions with neurons transduced to express the AstR. In horizontal slices of the medulla oblongata, electrical stimulation of Ast-3-expressing viscerosensory axons results in activity-dependent Ast-3 release and postsynaptic hyperpolarization of AstR-expressing NTS neurons. In conscious, freely moving animals expressing Ast-3 in viscerosensory afferents and AstR in postsynaptic NTS neurons, we observed a reduction in the sensitivity of the baroreceptor reflex that started 4 days after microinjection of the cNTS with the AstR-expressing virus and continued for the length of the experiment. This was associated with a transient pressor response. We also observed long-term alterations in bodyweight that were dependent upon bilateral transduction of vagal afferent neurons with Ast-3. Together, these observations substantiate an enhanced, highly specific chemogenetic approach that transforms the current

cardiac interbeat interval (IBI) (F), and the baroreceptor reflex sensitivity (BRS, G) derived from spontaneous fluctuations in sBP and IBI. These values were derived from analysis of 2h periods during the relatively inactive light period.

(H) In the schematic, green indicates the overlaid distribution of Lv-PRSx8-AstR-GFP (left) and Lv-PRSx8-GFP (right) transduced NTS neurons in all animals at a mid-level of the NTS. Complete maps are provided in Figure S5. Corresponding Ast-expressing vagal afferents (brown) are shown in the insets. The color intensity depicts increased overlap in distribution between animals in each group. Significant differences between groups were determined by RM two-way ANOVA with Bonferroni post hoc test, with bars denoting days with a difference and asterisks denoting $p < 0.05$. Abbreviations: 12N, hypoglossal nucleus; ST, solitary tract; AP, area postrema; DMV, dorsal motor nucleus of vagus; NTS, nucleus of the solitary tract.

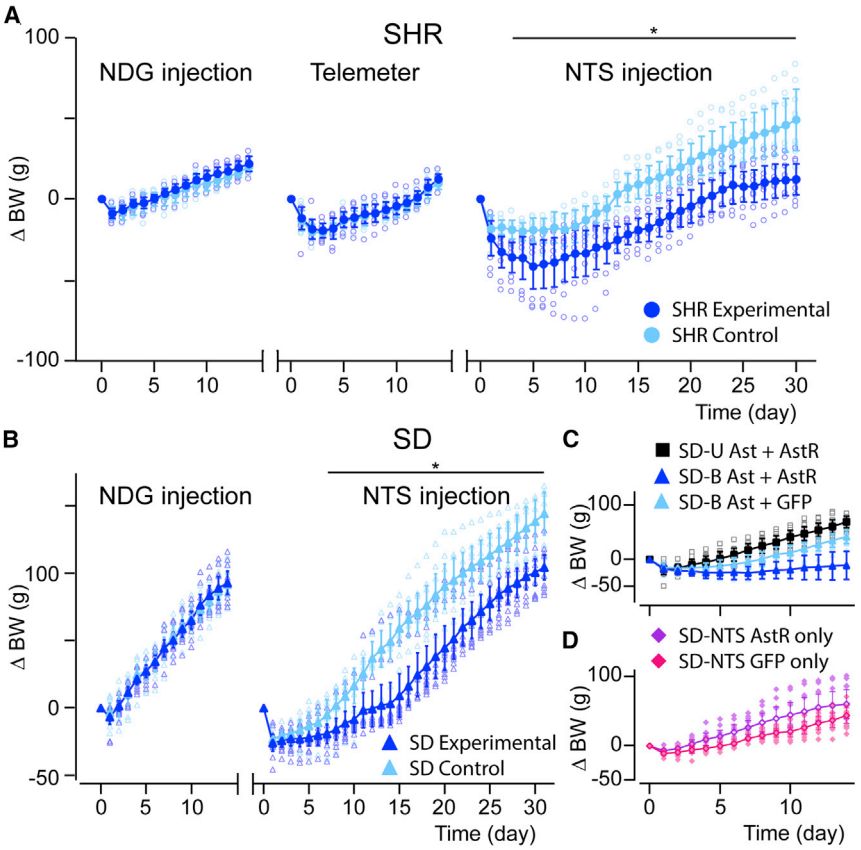


Figure 5. Effect of Inhibition of Vagal Viscerosensory Input to the Nucleus of the Solitary Tract on Bodyweight Homeostasis

(A–D) Graphs of change in bodyweight (Δ BW [g]) in the period following different, sequential surgeries in spontaneously hypertensive (SHR) (A) and Sprague-Dawley (SD) (B–D) rats. The group data are shown as mean ± 95% confidence interval in the closed symbols and the values for each individual rat as open symbols. In each graph, the x axis shows time with day 0 denoting the measurement on the day of surgery. The break in the axis depicts the period between each surgery.

(A) The SHR groups were treated identically for all surgeries where bilateral injections of rAAV1/2-HA-Ast-3-mCherry were made into the nodose ganglion (NDG injection) and then, ~2 weeks later, blood pressure telemeters were inserted into the abdominal aorta (Telemeter). In the final surgery, one group received microinjection of Lv-PRSx8-AstR-GFP in the nucleus of the solitary tract (NTS; SHR experimental; dark blue circles; n = 9) while the other received Lv-PRSx8-GFP (SHR control; light blue circles; n = 8).

(B) The SD rats were exposed to the same surgeries and viral injections but without the inclusion of blood pressure telemeters (SD. experimental; n = 10; dark blue triangles; SD. control; n = 10; light blue triangles).

(C) The data from the SD. experimental and SD. control rats were compared with a further control group in which the allatostatin virus was only injected unilaterally—these animals (n = 10) still received Lv-PRSx8-AstR-GFP in the NTS (black squares). There was no difference in the weight change between the unilateral rAAV1/2-HA-Ast-3-mCherry injected rats and the SD-control group.

(D) In another control experiment, the SD rats received only Lv-PRSx8-AstR-GFP (purple diamonds; n = 10) or Lv-PRSx8-GFP (magenta diamonds; n = 10) into the NTS and no NDG injections. There was no difference in the bodyweight change between these groups. Significant differences between groups were determined by RM two-way ANOVA with Bonferroni post hoc test, with bars denoting days with a difference and asterisks denoting $p < 0.05$.

chemogenetic toolkit by providing genetic expression of the activating ligand and the ability to interrogate specific pathways.

Chemogenetics using Ast was first described in 2002 (Lechner et al., 2002) and was shown to be a highly specific approach, due to the high-affinity interaction between the peptide ligand and its receptor. Because the peptide must be delivered behind the blood-brain barrier, the Ast approach has not gained the popularity of chemogenetics based around the mutated muscarinic receptor and clozapine-n-oxide—the DREADD system (Roth, 2016). Yet, several studies have demonstrated the utility of the Ast approach to inhibit tonically active neural pathways *in vivo* with powerful inhibition induced by activation of GIRK channels as well as inhibition of cAMP production (Lechner et al., 2002; Marina et al., 2011; Menuet et al., 2017; Tan et al., 2006). The viral-based Ast-3 expression system we have developed overcomes the hurdle related to delivery of Ast-3 to the brain, thus increasing the utility of Ast as a highly specific chemogenetic tool with no known off-target effects. We also provide proof of principle for the adoption of other peptidergic systems for chemogenetics, including ones that enable neural activation.

Effect on Baroreceptor Reflex Function

Arterial baroreceptor information is derived from vagal afferents with peripheral terminals in the aortic arch and glossopharyngeal afferents with terminals in the carotid sinus. Our transduction would only affect the aortic baroreceptors. Previous studies have concluded that bilateral surgical denervation of aortic arch baroreceptors induces detectable changes in baroreceptor reflex sensitivity (Osborn and England, 1990; Pickering et al., 2008). Such surgical denervation requires lesion of several nerves, including the superior cervical trunk, superior laryngeal nerve, and the aortic depressor nerve. The cervical vagus remains intact because animals do not survive bilateral lesions of the cervical vagus (Osborn and England, 1990). Thus, a specific, localized cessation of vagal afferent input bilaterally is not feasible with surgical methods. Here, our method allows demonstration of the effect of bilateral interruption of vagal afferent function. We observe reduced baroreceptor reflex sensitivity that develops within 4 days of microinjection of the AstR into the NTS and continues for the length of the recording period. Interestingly, the change in BP develops more slowly and is transient but reflects the time course of maximal inhibition of

baroreceptor reflex sensitivity. We propose that the time course is due to a combination of the time required for AAV transgene expression, which in most neural systems requires 2–4 weeks for maximal expression, and the complexity of the pathways contributing to homeostatic regulation of BP. Our approach will alter input from high-pressure aortic and low-pressure cardiac baroreceptors. Yet, the carotid baroreceptors remain intact and would be expected to compensate for loss of the aortic baroreceptors. The afferent pathways also affect neuroendocrine systems, in addition to the more rapidly acting neural autonomic pathways, and altered humoral regulation of blood pressure might be expected to develop over days.

Similar to aortic baroreceptor denervation, lesions of the NTS, which affect both aortic arch and carotid sinus baroreceptor input, reduce baroreceptor reflex sensitivity. Although there is evidence pointing to the involvement of A2 neurons in this response (Talman et al., 2012), whether this is due to altered afferent input to the TH-expressing neurons directly or to alterations in the integrating circuits in the NTS is not known. Here, we show the involvement of afferent input to Phox2-expressing neurons, of which the A2 neurons are a subset. This observation highlights the ability of this approach to further the understanding of neural circuits.

Effect on Bodyweight Homeostasis

We observe decreased bodyweight in response to Ast-3-mediated inhibition of Phox2-expressing neurons in the NTS, which was sustained for the length of the entire observation period. The involvement of the vagus nerve in modulating food intake has been studied extensively. Sub-diaphragmatic vagotomy, with varying levels of stomach resection or pylorectomy (Meyer, 1983), was performed as an early treatment for ulcers and associated with reduced bodyweight. Across multiple studies, the reduced bodyweight was considered the result of decreased food intake (Meyer, 1983). Inhibition of vagal activity with electrical vagal nerve block is approved by the Federal Drug Administration of the United States for use in obese humans. Although not effective in all studies (Sarr et al., 2012), vagal block reduced bodyweight and food intake in morbid and moderately obese humans (Camilleri et al., 2008; Morton et al., 2016; Shikora et al., 2016). In rats, lesions of the cNTS decrease bodyweight with a similar time course and magnitude to the one shown in this study (Hyde and Miselis, 1983; Menani et al., 1996). Input inhibition may reduce weight gain by increasing the sensitivity of satiating signals following food intake or decreasing hunger signals in experimental rats (Grill and Hayes, 2012). An association between vagal afferent activity and energy expenditure has also been reported (Liu et al., 2014), where deletion of peroxisome proliferator-activated receptor γ (PPARγ) from NDG neurons, which is associated with altered expression of excitatory synaptic markers, increased thermogenesis in response to high-fat diet (Liu et al., 2014). Overall, the data support a conclusion that the vagus nerve provides a hunger-promoting signal in humans and experimental animals, via mechanisms that need to be fully elucidated.

A proportion of the cNTS neurons transduced with AstR and receiving an Ast-3 input was A2 noradrenergic neurons. These neurons have complex effects on bodyweight, with the activity of some A2 neurons increasing with meal size (Kreisler et al., 2014), and lesions of A2 neurons, suggesting that they convey the satiety signal induced by cholecystokinin (Rinaman, 2003). Supporting this, activation of A2 neurons projecting to the parabrachial nucleus decreases food intake (Roman et al., 2016). Inhibition of vagal afferent excitation of these neurons should increase bodyweight. Yet, another population of cNTS A2 neurons projects to the arcuate nucleus to increase feeding (Aklan et al., 2020), and decreased excitation of these would decrease bodyweight. Here, we observed that bilateral release of Ast-3 from viscerosensory neurons synapsing with Phox2-expressing NTS neurons reduces bodyweight gain in both SHR and SD rats. Our hypothesis is that different populations of A2 neurons will receive different vagal sensory information and affect bodyweight control appropriately—the overall influence, under basal conditions, is to drive feeding, but this likely changes with state, such as in obesity (Wall et al., 2019).

Potential Caveats Associated with Transgene Expression

The most likely explanation for our physiological observations involves inhibition of NTS neurons receiving the vagal afferent input; however, we also induced expression of the AstR in many cholinergic neurons in the DMV and, to a lesser degree, neurons in the AP. The vagal afferent input to the DMV is relatively sparse but is readily apparent, and many of the AstR-expressing DMV neurons exhibit close appositions with Ast-3-expressing vagal afferents. Although the effect of direct vagal afferent input to vagal efferent neurons is not known, and even the overall effect of altered vagal efferent activity on bodyweight remains unclear (Browning and Travagli, 2014), we think this pathway is unlikely to account for our physiological observations. Modulation of DMV vagal efferent neuron activity alters ventricular contractility (Machhada et al., 2015), and although contractility was not directly examined in this study, we did not observe any overt effects on cardiac function. Direct stimulation of DMV neurons decreases food intake and bodyweight (NamKoong et al., 2019), while lesions of the cNTS, which reduce bodyweight to a similar degree to the results of this study, do not alter intestinal transit time or gastric retention. Together, the data indicate that the decreased bodyweight is unlikely to be due to altered vagal efferent motor function (Hyde and Miselis, 1983). We also observed Ast-3-expressing afferents in the AP, which has been implicated in bodyweight regulation (Wang and Edwards, 1997) and paratrigeminal nucleus; however, these regions are unlikely to contribute to the bodyweight phenotype we observed because very few of these neurons in these regions also expressed the AstR.

Technical Limitations

The genetic expression of Ast-3 is a highly valuable characteristic of this system and cannot be achieved for the activating "ligands" for either optogenetics or the other current chemogenetic systems. Being able to express the ligand in defined cell groups and obtain activity-dependent synaptic release will enhance other research areas. The ability to express the receptor in another defined, specific cell group enables a plethora of experimental manipulations that interrogate the connections of tonically active cell groups.

Benchmarking a technical development against accepted methods is key. We discuss the validation of this approach by comparison with previously published data using surgical methods to lesion viscerosensory nerves or the NTS. Direct comparison with another chemogenetic approach would be valuable, but the increased specificity of our approach makes this difficult. Within the viscerosensory system, we altered the synaptic excitatory drive of active afferents to include sustained inhibition. This is not likely to be continuous but effective only during periods of afferent activation. To date, no DREADD chemogenetic studies have attempted such temporal control of inhibition. In addition, our approach will only inhibit the synapse between presynaptic and postsynaptic neurons that have been transduced. Even though our NTS injections will transduce many neurons with the AstR, including second- and higher-order neurons, only those receiving active input from transduced afferents will be affected—this is likely to be a subset of second-order neurons. Obtaining such circuit specificity cannot be mimicked by other chemogenetic approaches, and thus, *in vivo* validation against accepted approaches is problematic.

Despite these benefits, some caveats need to be considered. Our results indicate that Ast-3 will be released from highly active neurons. In whole-cell patch-clamp experiments, stimulation of vagal afferents at 50 Hz for 30 s induced postsynaptic hyperpolarization. Although not systematically studied, in one responsive neuron that could be held for long enough to examine another stimulation parameter, 20 Hz stimulation for 30 s also evoked hyperpolarization. Stimulation at 50 Hz stimulation for 2 s did not evoke hyperpolarization in four cells where this was tested (data not shown). These stimulation parameters would be congruent with Ast being packaged in large, dense core vesicles, as has been for other neurophysin-directed peptidergic systems (Zhang et al., 2005). Accordingly, Ast-3 release might not occur in neurons that do not fire at high frequencies for prolonged time periods. In intermittently firing or temporally modulated neurons, release might occur selectively during periods of high activity. We suggest that the requirement of high-frequency, action-potential-dependent release could represent either an advantage, or limitation, depending on the functional properties of the specific pathway being examined. In an inactive pathway, it is possible that the Ast-3 expression could be combined with co-expression of an activating molecule, such as channelrhodopsin, thus giving the ability to interrogate the function of a pathway. Although the release of Ast-3 provides information about a particular neural pathway, loss of function in this paradigm does not prove full dependency to elicit function. The activation of the AstR leads to hyperpolarization of the recipient neuron, presumably making it less responsive to any other inputs. Finally, although we demonstrate action-potential-dependent hyperpolarization of AstR-expressing neurons without effect on non-AstR-expressing cells, we cannot rule out the possibility of non-synaptic or volume transmission effects of Ast-3.

Conclusions

We describe a chemogenetic approach involving the highly selective interaction between the insect peptide Ast-3 and its AstR, both of which are inert in mammals. Using neuronal expression of Ast-3, we overcome issues associated with delivering Ast into the brain and extend chemogenetics to enable chronic interrogation of active circuits in conscious, freely moving animals. This proof of principle opens the possibility to transducing other cell types, such as choroid plexus, to enable delivery of Ast-3 to the brain and potentially with temporal control. We validate both the expression and physiological function of this chemogenetic approach within the vagal viscerosensory system, reproducing known effects on baroreceptor and bodyweight homeostasis but also gaining insights into the cellular basis of these regulatory systems. We propose that this enhanced Ast-3/AstR system has broad application within many areas of neuroscience research requiring an activity-dependent, circuit-based, chemogenetic toolkit.

STAR★METHODS

Detailed methods are provided in the online version of this paper and include the following:

- KEY RESOURCES TABLE
- RESOURCE AVAILABILITY
  - Lead Contact
  - Materials Availability
  - Data and Code Availability
- EXPERIMENTAL MODEL AND SUBJECT DETAILS
  - Animals
  - Cell lines
- METHOD DETAILS
  - Plasmids
  - Cell culture and transfection for *in vitro* bioassays
  - Viral production – recombinant adeno-associated virus 1/2-HA-Ast-3-mCherry
  - Recombinant adeno-associated virus purification and viral titration
  - Viral production - Lentivirus
  - Production of CHO-AstR cells
  - Measurement of cAMP
  - Synthetic peptides
  - *In vivo* validation - General surgical procedures
  - Injections into the nodose ganglion
  - Injections into the nucleus of the solitary tract
  - Protocols
  - Patch clamp recordings of transduced NTS neurons in slices
  - Expression of rAAV1/2-HA-Ast-3-mCherry in nodose ganglion and Lv-PRSx8-AstR or Lv-PRSx8-GFP in NTS of blood pressure telemetered SHR
  - Expression of rAAV1/2-HA-Ast-3-mCherry in nodose ganglion and Lv-PRSx8-AstR in NTS of SD rats
  - Tissue perfusion
  - Immunohistochemistry
  - Nodose ganglia
  - Brainstem sections
  - Microscopy
  - Mapping of transduced neurons in the nucleus of the solitary tract
- QUANTIFICATION AND STATISTICAL ANALYSIS

SUPPLEMENTAL INFORMATION

Supplemental Information can be found online at https://doi.org/10.1016/j.celrep.2020.108139.

ACKNOWLEDGMENTS

We are very grateful to Tania Ferraro for assistance with assays and Jairus Bowne for generating schematic diagrams. Grant funding was provided by the Australian NHMRC (APP#1102477 and APP#1156727), the Australian Research Council (DP170104582), and the State Government of Victoria Operational Infrastructure Support Program to the Florey Institute. R.A.D.B. is an NHMRC Senior Research Fellow.

AUTHOR CONTRIBUTIONS

Conceptualization, R.A.D.B. and A.M.A.; Methodology, S.L., A.A.C., J.K.B., S.J.M., M.R.M., R.A.D.B., and A.M.A.; Software, L.X.; Validation, M.R.M., S.J.M., R.A.D.B., and A.M.A.; Formal Analysis, H.B.N., M.R.M., L.X., C.M., S.J.M., R.A.D.B., and A.M.A.; Investigation, H.B.N., M.R.M., S.L., A.A.C., J.K.B., and S.J.M.; Writing – Original Draft, H.B.N., S.J.M., R.A.D.B., and A.M.A.; Writing – Reviewing & Editing, H.B.N., M.R.M., J.K.B., C.M., S.J.M., R.A.D.B., and A.M.A.; Visualization, H.B.N., M.R.M., A.A.C., C.M., S.J.M., R.A.D.B., and A.M.A.; Supervision, R.A.D.B. and A.M.A.; Project Administration, R.A.D.B. and A.M.A.; Funding Acquisition, R.A.D.B. and A.M.A.

DECLARATION OF INTERESTS

The authors declare no competing interests.

Received: May 11, 2020
Revised: July 2, 2020
Accepted: August 21, 2020
Published: September 15, 2020

REFERENCES

Aklan, I., Sayar Atasoy, N., Yavuz, Y., Ates, T., Coban, I., Koksalar, F., Filiz, G., Topcu, I.C., Oncul, M., Dilsiz, P., et al. (2020). NTS Catecholamine Neurons Mediate Hypoglycemic Hunger via Medial Hypothalamic Feeding Pathways. Cell Metab. *31*, 313–326.

Andresen, M.C., Doyle, M.W., Jin, Y.H., and Bailey, T.W. (2001). Cellular mechanisms of baroreceptor integration at the nucleus tractus solitarius. Ann. N Y Acad. Sci. *940*, 132–141.

Bathgate, R.A., Lin, F., Hanson, N.F., Otvos, L., Jr., Guidolin, A., Giannakis, C., Bastiras, S., Layfield, S.L., Ferraro, T., Ma, S., et al. (2006). Relaxin-3: improved synthesis strategy and demonstration of its high-affinity interaction with the relaxin receptor LGR7 both in vitro and in vivo. Biochemistry *45*, 1043–1053.

Ben-Barak, Y., Russell, J.T., Whitnall, M.H., Ozato, K., and Gainer, H. (1985). Neurophysin in the hypothalamo-neurohypophysial system. I. Production and characterization of monoclonal antibodies. J. Neurosci. *5*, 81–97.

Bendena, W.G., Garside, C.S., Yu, C.G., and Tobe, S.S. (1997). Allatostatins: diversity in structure and function of an insect neuropeptide family. Ann. N Y Acad. Sci. *814*, 53–66.

Birgül, N., Weise, C., Kreienkamp, H.J., and Richter, D. (1999). Reverse physiology in Drosophila: identification of a novel allatostatin-like neuropeptide and its cognate receptor structurally related to the mammalian somatostatin/galanin/opioid receptor family. EMBO J. *18*, 5892–5900.

Browning, K.N., and Travagli, R.A. (2014). Central nervous system control of gastrointestinal motility and secretion and modulation of gastrointestinal functions. Compr. Physiol. *4*, 1339–1368.

Callander, G.E., Ma, S., Ganella, D.E., Wimmer, V.C., Gundlach, A.L., Thomas, W.G., and Bathgate, R.A. (2012). Silencing relaxin-3 in nucleus incertus of adult rodents: a viral vector-based approach to investigate neuropeptide function. PLoS ONE *7*, e42300.

Camilleri, M., Toouli, J., Herrera, M.F., Kulseng, B., Kow, L., Pantoja, J.P., Marvik, R., Johnsen, G., Billington, C.J., Moody, F.G., et al. (2008). Intra-abdominal vagal blocking (VBLOC therapy): clinical results with a new implantable medical device. Surgery *143*, 723–731.

Card, J.P., Lois, J., and Sved, A.F. (2010). Distribution and phenotype of Phox2a-containing neurons in the adult sprague-dawley rat. J. Comp. Neurol. *518*, 2202–2220.

Chang, L.J., Urlacher, V., Iwakuma, T., Cui, Y., and Zucali, J. (1999). Efficacy and safety analyses of a recombinant human immunodeficiency virus type 1 derived vector system. Gene Ther. *6*, 715–728.

Chen, D., Bassi, J.K., Walther, T., Thomas, W.G., and Allen, A.M. (2010). Expression of angiotensin type 1A receptors in C1 neurons restores the sympathoexcitation to angiotensin in the rostral ventrolateral medulla of angiotensin type 1A knockout mice. Hypertension *56*, 143–150.

Dauger, S., Pattyn, A., Lofaso, F., Gaultier, C., Goridis, C., Gallego, J., and Brunet, J.F. (2003). Phox2b controls the development of peripheral chemoreceptors and afferent visceral pathways. Development *130*, 6635–6642.

Deisseroth, K. (2015). Optogenetics: 10 years of microbial opsins in neuroscience. Nat. Neurosci. *18*, 1213–1225.

Gomez, J.L., Bonaventura, J., Lesniak, W., Mathews, W.B., Sysa-Shah, P., Rodriguez, L.A., Ellis, R.J., Richie, C.T., Harvey, B.K., Dannals, R.F., et al. (2017). Chemogenetics revealed: DREADD occupancy and activation via converted clozapine. Science *357*, 503–507.

Grill, H.J., and Hayes, M.R. (2012). Hindbrain neurons as an essential hub in the neuroanatomically distributed control of energy balance. Cell Metab. *16*, 296–309.

Grimm, D., Kay, M.A., and Kleinschmidt, J.A. (2003). Helper virus-free, optically controllable, and two-plasmid-based production of adeno-associated virus vectors of serotypes 1 to 6. Mol. Ther. *7*, 839–850.

Huang, X., Hartley, A.V., Yin, Y., Herskowitz, J.H., Lah, J.J., and Ressler, K.J. (2013). AAV2 production with optimized N/P ratio and PEI-mediated transfection results in low toxicity and high titer for in vitro and in vivo applications. J. Virol. Methods *193*, 270–277.

Hyde, T.M., and Miselis, R.R. (1983). Effects of area postrema/caudal medial nucleus of solitary tract lesions on food intake and body weight. Am. J. Physiol. *244*, R577–R587.

Ivell, R., and Richter, D. (1984). Structure and comparison of the oxytocin and vasopressin genes from rat. Proc. Natl. Acad. Sci. USA *81*, 2006–2010.

Kreisler, A.D., Davis, E.A., and Rinaman, L. (2014). Differential activation of chemically identified neurons in the caudal nucleus of the solitary tract in non-entrained rats after intake of satiating vs. non-satiating meals. Physiol. Behav. *136*, 47–54.

Kuusela, T. (2013). Methodological aspects of baroreflex sensitivity analysis. In Heart Rate Variability (HRV) Signal Analysis: Clinical Applications, M.V. Kamath, M.A. Watanabe, and A.R.M. Upton, eds. (CRC Press), pp. 43–58.

Lechner, H.A., Lein, E.S., and Callaway, E.M. (2002). A genetic method for selective and quickly reversible silencing of Mammalian neurons. J. Neurosci. *22*, 5287–5290.

Liu, C., Bookout, A.L., Lee, S., Sun, K., Jia, L., Lee, C., Udit, S., Deng, Y., Scherer, P.E., Mangelsdorf, D.J., et al. (2014). PPARγ in vagal neurons regulates high-fat diet induced thermogenesis. Cell Metab. *19*, 722–730.

Machhada, A., Ang, R., Ackland, G.L., Ninkina, N., Buchman, V.L., Lythgoe, M.F., Trapp, S., Tinker, A., Marina, N., and Gourine, A.V. (2015). Control of ventricular excitability by neurons of the dorsal motor nucleus of the vagus nerve. Heart Rhythm *12*, 2285–2293.

Marina, N., Abdala, A.P., Korsak, A., Simms, A.E., Allen, A.M., Paton, J.F., and Gourine, A.V. (2011). Control of sympathetic vasomotor tone by catecholaminergic C1 neurones of the rostral ventrolateral medulla oblongata. Cardiovasc. Res. *91*, 703–710.

Menani, J.V., Colombari, E., Talman, W.T., and Johnson, A.K. (1996). Commissural nucleus of the solitary tract lesions reduce food intake and body weight gain in rats. Brain Res. *740*, 102–108.

Menuet, C., Le, S., Dempsey, B., Connelly, A.A., Kamar, J.L., Jancovski, N., Bassi, J.K., Walters, K., Simms, A.E., Hammond, A., et al. (2017). Excessive Respiratory Modulation of Blood Pressure Triggers Hypertension. Cell Metab. *25*, 739–748.

Meyer, J.H. (1983). Chronic morbidity after ulcer surgery. In Gastrointestinal Disease: Pathophysiology, Diagnosis, Management, M.H. Sleisenger and J.H. Fordtran, eds. (W.B. Saunders Co.), pp. 757–779.

Morton, J.M., Shah, S.N., Wolfe, B.M., Apovian, C.M., Miller, C.J., Tweden, K.S., Billington, C.J., and Shikora, S.A. (2016). Effect of Vagal Nerve Blockade on Moderate Obesity with an Obesity-Related Comorbid Condition: the ReCharge Study. Obes. Surg. *26*, 983–989.

NamKoong, C., Song, W.J., Kim, C.Y., Chun, D.H., Shin, S., Sohn, J.W., and Choi, H.J. (2019). Chemogenetic manipulation of parasympathetic neurons (DMV) regulates feeding behavior and energy metabolism. Neurosci. Lett. *712*, 134356.

Osborn, J.W., and England, S.K. (1990). Normalization of arterial pressure after barodenervation: role of pressure natriuresis. Am. J. Physiol. *259*, R1172–R1180.

Osborn, J.W., and Hornfeldt, B.J. (1998). Arterial baroreceptor denervation impairs long-term regulation of arterial pressure during dietary salt loading. Am. J. Physiol. *275*, H1558–H1566.

Paxinos, G., and Watson, C. (2006). The Rat Brain in Stereotaxic Coordinates (Elsevier Science).

Pickering, A.E., Simms, A.E., and Paton, J.F. (2008). Dominant role of aortic baroreceptors in the cardiac baroreflex of the rat in situ. Auton. Neurosci. *142*, 32–39.

Rao, V.V., Löffler, C., Battey, J., and Hansmann, I. (1992). The human gene for oxytocin-neurophysin I (OXT) is physically mapped to chromosome 20p13 by in situ hybridization. Cytogenet. Cell Genet. *61*, 271–273.

Rinaman, L. (2003). Hindbrain noradrenergic lesions attenuate anorexia and alter central cFos expression in rats after gastric viscerosensory stimulation. J. Neurosci. *23*, 10084–10092.

Robertson, D., Hollister, A.S., Biaggioni, I., Netterville, J.L., Mosqueda-Garcia, R., and Robertson, R.M. (1993). The diagnosis and treatment of baroreflex failure. N. Engl. J. Med. *329*, 1449–1455.

Roman, C.W., Derkach, V.A., and Palmiter, R.D. (2016). Genetically and functionally defined NTS to PBN brain circuits mediating anorexia. Nat. Commun. *7*, 11905.

Roth, B.L. (2016). DREADDs for Neuroscientists. Neuron *89*, 683–694.

Sarr, M.G., Billington, C.J., Brancatisano, R., Brancatisano, A., Toouli, J., Kow, L., Nguyen, N.T., Blackstone, R., Maher, J.W., Shikora, S., et al.; EMPOWER Study Group (2012). The EMPOWER study: randomized, prospective, double-blind, multicenter trial of vagal blockade to induce weight loss in morbid obesity. Obes. Surg. *22*, 1771–1782.

Shikora, S.A., Toouli, J., Herrera, M.F., Kulseng, B., Brancatisano, R., Kow, L., Pantoja, J.P., Johnsen, G., Brancatisano, A., Tweden, K.S., et al. (2016). Intermittent Vagal Nerve Block for Improvements in Obesity, Cardiovascular Risk Factors, and Glycemic Control in Patients with Type 2 Diabetes Mellitus: 2-Year Results of the VBLOC DM2 Study. Obes. Surg. *26*, 1021–1028.

Stornetta, R.L., Moreira, T.S., Takakura, A.C., Kang, B.J., Chang, D.A., West, G.H., Brunet, J.F., Mulkey, D.K., Bayliss, D.A., and Guyenet, P.G. (2006). Expression of Phox2b by brainstem neurons involved in chemosensory integration in the adult rat. J. Neurosci. *26*, 10305–10314.

Talman, W.T., Dragon, D.N., Jones, S.Y., Moore, S.A., and Lin, L.H. (2012). Sudden death and myocardial lesions after damage to catecholamine neurons of the nucleus tractus solitarii in rat. Cell. Mol. Neurobiol. *32*, 1119–1126.

Tan, E.M., Yamaguchi, Y., Horwitz, G.D., Gosgnach, S., Lein, E.S., Goulding, M., Albright, T.D., and Callaway, E.M. (2006). Selective and quickly reversible inactivation of mammalian neurons in vivo using the Drosophila allatostatin receptor. Neuron *51*, 157–170.

Wall, K.D., Olivos, D.R., and Rinaman, L. (2019). High Fat Diet Attenuates Cholecystokinin-Induced cFos Activation of Prolactin-Releasing Peptide-Expressing A2 Noradrenergic Neurons in the Caudal Nucleus of the Solitary Tract. Neuroscience, Published online September 10, 2019. https://doi.org/10.1016/j.neuroscience.2019.08.054.

Wang, T., and Edwards, G.L. (1997). Differential effects of dorsomedial medulla lesion size on ingestive behavior in rats. Am. J. Physiol. *273*, R1299–R1308.

Williams, E.K., Chang, R.B., Strochlic, D.E., Umans, B.D., Lowell, B.B., and Liberles, S.D. (2016). Sensory Neurons that Detect Stretch and Nutrients in the Digestive System. Cell *166*, 209–221.

Zeng, W.Z., Marshall, K.L., Min, S., Daou, I., Chapleau, M.W., Abboud, F.M., Liberles, S.D., and Patapoutian, A. (2018). PIEZOs mediate neuronal sensing of blood pressure and the baroreceptor reflex. Science *362*, 464–467.

Zhang, B.J., Yamashita, M., Fields, R., Kusano, K., and Gainer, H. (2005). EGFP-tagged vasopressin precursor protein sorting into large dense core vesicles and secretion from PC12 cells. Cell. Mol. Neurobiol. *25*, 581–605.

Zolotukhin, S., Byrne, B.J., Mason, E., Zolotukhin, I., Potter, M., Chesnut, K., Summerford, C., Samulski, R.J., and Muzyczka, N. (1999). Recombinant adeno-associated virus purification using novel methods improves infectious titer and yield. Gene Ther. *6*, 973–985.

CellPress
OPEN ACCESS

STAR★METHODS

KEY RESOURCES TABLE

REAGENT or RESOURCE	SOURCE	IDENTIFIER
Antibodies		
Goat anti-choline acetyltransferase (1:2,000)	Chemicon, Australia,	Lot: 2661265, Cat: AB144P, RRID: AB_2079751
Rabbit anti-dsRed (1:2,000 (NDG), 1:5,000 (medulla))	Takara Bio, Clontech, Australia	Lot: 1805060, Cat:632496, RRID: AB_10013483
Goat anti-mCherry (1:2,000 (NDG))	Scigen, Portugal	Cat: AB0040-200, RRID: AB_2333092
Chicken anti-GFP (1:5,000)	Abcam, Australia	Lot: GR23665-17, Cat: AB13970, RRID: AB_300798
Mouse anti-hemagglutinin tag (1:5,000)	Biolegend, USA	Lot: B269834, Cat:901501, RRID: AB_2565006
Rabbit anti-hemagglutinin tag (1:2,500 (NDG))	Rockland, USA	Lot: 12289, Cat: 600-401-384, RRID: AB_217929
Mouse anti-neurophysin I (1:1,500 (NDG), 1:2,000 (medulla))	Millipore, Australia	Lot: Q2586374, Cat: MABN844; Ben-Barak et al., 1985
Mouse anti-tyrosine hydroxylase (1:5,000)	Millipore, Australia	Lot: 3083054, Cat: MAB318, RRID: AB_2201528
Alexa488-conjugated donkey anti-chicken IgG (1:500)	Jackson ImmunoResearch Laboratories, USA	Lot:133645, Cat: 703545155, RRID: AB_2340375
Cy3-conjugated donkey anti-goat IgG (1:500)	Jackson ImmunoResearch Laboratories, USA	Lot:87377, Cat: 705165003, RRID: AB_2340411
Cy5-conjugated donkey anti-goat IgG (1:200)	Jackson ImmunoResearch Laboratories, USA	Lot:124689, Cat: 705175147, RRID: AB_2340415
Cy5-conjugated donkey anti-mouse (1:200 (NDG), 1:500 (medulla))	Jackson ImmunoResearch Laboratories, USA	Lot:120906, Cat: 715175151, RRID: AB_2340820
Cy3-conjugated donkey anti-rabbit (1:200 (NDG), 1:500 (medulla))	Jackson ImmunoResearch Laboratories, USA	Lot:133645, Cat: 711165152, RRID: AB_2307443;
Alexa488-conjugated donkey anti-rabbit (1:200)	Jackson ImmunoResearch Laboratories, USA	Lot:127725, Cat: 711545152, RRID: AB_2313584
Bacterial and Virus Strains		
Stbl3 chemically competent *E. coli*	ThermoFisher Scientific, Australia	Cat: C737303
rAAV1/2-HA-Ast-3-mCherry ($5.08x10^{11}$ genome copies/mL)	This paper	N/A
Lv-PRSx8-AstR-p2A-GFP (3.76×10^9 infectious units/mL)	Generated in the Allen laboratory	Chen et al., 2010
Lv-PRSx8-GFP (6.9×10^9 infectious units/mL)	Generated in the Allen laboratory	Chen et al., 2010
Chemicals, Peptides, and Recombinant Proteins		
Allatostatin	GL Biochem Ltd, China	Custom synthesis
HA-allatostatin	GL Biochem Ltd, China	Custom synthesis
Experimental Models: Cell Lines		
Human embryonic kidney 293 T cells (HEK293T)	American Type Culture Collection, USA	CRL-3216
Human embryonic kidney 293 FT cells (HEK293FT)	ThermoFisher Scientific, Australia	R70007
Chinese Hamster ovarian cells (CHO-K1)	American Type Culture Collection, USA	CCL-61
Stable transfected CHO-K1-AstR-GFP cells	This paper	N/A

(*Continued on next page*)

Continued

REAGENT or RESOURCE	SOURCE	IDENTIFIER
Experimental Models: Organisms/Strains		
Spontaneously Hypertensive Rats	Animal Resources Centre, Canning Vale, West Australia, Australia	N/A
Sprague Dawley Rats	Biological Resources Facility, University of Melbourne, Melbourne, Victoria, Australia	N/A
Oligonucleotides		
HA-Ast-3 primer: forward: 5′-CATC ATCATGGATCCACCAT GGCC TGCCCCAGT CTTG-3′	This paper	N/A
HA-Ast-3 primer: reverse: 5‘-CATC ATCATGAATT CTTACTTGTACAG CTCGTCCATGC-3′	This paper	N/A
Recombinant DNA		
pBHA cloning vector	Bioneer Corporation, Republic of South Korea	Cat# K-7110
pAM-DCA-spe-tdTomato	Kind gift from V.C. Wimmer, Florey Institute of Neuroscience and Mental Health	Callander et al., 2012 Original derivation: Grimm et al., 2003
pDPI	Kind gift from V.C. Wimmer, Florey Institute of Neuroscience and Mental Health	Original derivation: Grimm et al., 2003
pDPII	Kind gift from V.C. Wimmer, Florey Institute of Neuroscience and Mental Health	Original derivation: Grimm et al., 2003
pAM-DCA-HA-Ast-3-NP-1-IRES-mCherry-WPRE (AddGene #159630)	This paper	N/A
pCSC-CMV-HA-Ast-3-NP-1-IRES-mCherry (AddGene #159631)	This paper	N/A
pTYF-PRSx8-AstR-p2A-GFP (AddGene #159632)	Generated in the Allen laboratory	Chen et al., 2010
pAAV-hSyn-AstR-IRES-GFP	Kind gift from J.L. Feldman, UCLA, USA.	Tan et al., 2006
pTYF-CBA-AstR-IRES-GFP	This paper	N/A
pMDL	Kind gift from S. Kasparov, University of Bristol, UK	Original derivation: Chang et al., 1999
pRSV	Kind gift from S. Kasparov, University of Bristol, UK	Original derivation: Chang et al. 1999
pCMV-VSV-G	Kind gift from S. Kasparov, University of Bristol, UK	Original derivation: Chang et al., 1999
Software and Algorithms		
Cell Quest (version 5.1)	BD Biosciences, Australia	N/A
Spike 2 (version 9)	Cambridge Electronic Design, UK	N/A
Baroreflex sensitivity custom script (MATLAB)	This paper	N/A
Zen (Black edition SP1, version 8.1, 2012)	Zeiss, Australia	N/A
Photoshop (CC 2020)	Adobe, USA	N/A
Illustrator (CC 2020)	Adobe, USA	N/A
Inkscape (version 0.92.4, 2019)	Inkscape	N/A
GraphPad Prism (version 8.1)	GraphPad Inc., USA	N/A

RESOURCE AVAILABILITY

Lead Contact

Further information and requests for resources or reagents should be direct to, and will be fulfilled by, the Lead Contact, Andrew M. Allen (a.allen@unimelb.edu.au).

CellPress
OPEN ACCESS

Materials Availability

Plasmids generated in this study will be made available from AddGene. Stably transfected cell lines are available, upon request, from the Lead Contact.

Data and Code Availability

All the data that support the findings of this study are available from the Lead Contact upon reasonable request. The code written for measurement of baroreceptor reflex sensitivity is available upon request to the Lead Contact.

EXPERIMENTAL MODEL AND SUBJECT DETAILS

Animals

All animal work was approved by the University of Melbourne Animal Ethics Committee (Approval Number: 1614877), and carried out in accordance with the National Health & Medical Research Council of Australia guidelines; 2004 *Australian code of practice for the Care and use of Animals for Scientific Purposes* and 2008 *Guidelines to Promote the Wellbeing of Animals Used for Scientific Purposes*. All *in vivo* experiments used male rats obtained at approximately 6 weeks of age. Sprague Dawley (SD) rats were bred at the Biological Resources Facility of the University of Melbourne. Spontaneously Hypertensive rats (SHR) were purchased from the Animal Resource Centre (Canning Vale, Australia). Rats were group housed with littermates, with the exception of a 24 h period post-surgery when they were housed singly, in standard cages at a constant temperature (22 ± 1°C), and maintained on a 12h light:dark cycle (lights on from 6 A.M. to 6 P.M.) with *ad libitum* access to standard chow and water. Rats were randomly assigned to the experimental or control group at the start of the protocol.

Cell lines

Human embryonic kidney 293 cell containing the SV40 T-antigen (HEK293T) and Chinese Hamster ovarian cell (CHO-K1) were sourced from ATCC (CRL-3216 and CCL-61 respectively). Another human embryonic kidney 293 cell line containing the SV40 T-antigen (HEK293FT) was sourced from ThermoFisher Scientific, Australia (R70007). Before use cells were maintained in liquid nitrogen. All cell lines were maintained at 37°C with 5% CO_2 in 50% Dulbecco's modified Eagle's medium and 50% Ham's F12 (Invitrogen, Australia), supplemented with 10% fetal bovine serum, 100 μg/mL penicillin, 100 μg/mL streptomycin and 2 mM L-glutamine (Invitrogen; complete DMEM media). Cells were maintained at 40%–50% confluency for passaging and washed with warm PBS and split with trypsin/EDTA. The cell lines were tested monthly and were mycoplasma free.

METHOD DETAILS

Plasmids

All plasmid and transgenic protocols were approved by the Institutional Biosafety Committees in accordance with the guidelines from the Office of Gene Technology Regulator (NLRD-8890; Australian Government). The allatostatin precursor construct was synthesized using the mammalian oxytocin (OXT) sequence, including the signal peptide, amidation motif and neurophysin-1 sequence as a template (Figure S1A). The OXT sequence was replaced by the HA-Ast-3 sequence and the gene synthesized in a cloning vector pBHA (vector primer: pBA_F/pBH_R; Bioneer Corporation, Daejeon, Republic of South Korea). The sequence was cloned into the recombinant adeno associated virus (rAAV) 1/2 vector pAM-DCA-spe-tdTomato (kindly provided by Dr Verena Wimmer, Florey Institute of Neuroscience and Mental Health, Melbourne, VIC, Australia) (Callander et al., 2012) by a three-stage cloning process to produce pAM-DCA-HA-Ast-3-IRES-mCherry (pAM-HA-Ast-3-mCherry; Figure S1B; AddGene #159630). Initially, the Ast-3 precursor was cloned into a lentivirus as an intermediate vector to obtain IRES-mCherry, as cloning into the rAAV1/2 expression vector results in the excision of tdTomato. A mammalian expression vector, pcDNA3.1zeo (+)-Ast, and recipient lentivirus, pCSC-CMV-IRES-mCherry, was double digested with BamHI and XhoI to release the insert (441 base pair) which was ligated to produce pCSC-CMV-HA-Ast-3-IRES-mCherry. The coding region of the Ast-3-IRES-mCherry sequence was then PCR amplified, to obtain restriction sites for cloning into the rAAV1/2 vector from the lentivirus vector (pCSC-CMV-HA-Ast-3-IRES-mCherry; AddGene #159631) using a forward primer introducing a BamHI restriction site at the 5' end (5′-CATCATCATGGATCCACCAT GGCCTGCCCCAGT CTTG-3′) and a reverse primer introducing an EcoRI restriction site at the 3' end (5'-CATCATCATGAATT CTTACTTGTACAGCTCGTCCATGC-3′). The PCR product was run on a 1% agarose gel confirming the size of the product (HA-Ast-3-IRES-mCherry, 1700 base pair) and then gel purified using a Wizard spin column gel purification kit (Promega, USA). The insert was then cloned into the expression vector, pAM-DCA-spe-tdTomato. The tdTomato was excised using a double digestion of BamHI and EcoRI, followed by treatment with thermosensitive alkaline phosphatase to dephosphorylate the 5' end and prevent re-ligation. HA-Ast-3-IRES-mCherry was ligated into the pAM vector to produce pAM-HA-Ast-3-mCherry which contained a chicken β-actin, chicken β-actin/cytomegalovirus hybrid promoter (DCA), a downstream internal ribosome entry site (IRES) followed by the sequence for the fluorophore, mCherry, and a Woodchuck-Hepatitis Virus post-transcriptional regulatory element (WPRE). Control plasmid experiments used a mammalian expression vector (pcDNA3.1zeo (+)).

All ligations were performed at 4°C overnight with T4 ligase and ligation products were transformed into stbl3 competent cells (Thermofisher Scientific) and plated onto Luriabroth agar plates containing ampicillin. Colonies were selected and DNA was

extracted from the cultures and purified using a Miniprep kit (QIAGEN, Australia) followed by digestion analysis to confirm inserts. All clones were sequenced on both strands of DNA to ensure no addition, deletion or substitution in the DNA sequence. Final clones with the correct sequence underwent large scale production of DNA through Maxiprep kit (QIAGEN) and DNA was stored at 20°C for use in *in vitro* analysis and rAAV production.

Cell culture and transfection for *in vitro* bioassays

HEK293T cells were seeded at 60%–70% confluency one day prior to transfection using plasmid DNA, Lipofectamine2000 (ThermoFisher Scientific, Australia) and Opti-MEM reduced serum media (ThermoFisher Scientific). The cells were seeded at 600,000 cells per well (6 well plate) for studies examining secretion of bioactive peptide. CHO-K1 cells were seeded at 8,000 cells per well (96-well plate) one day prior to transfection for short term experiments. Transient co-transfection of CHO-K1 cells was performed using Viafect (Promega, USA) as per the manufacturer's instructions. Plasmid DNA with Viafect was made up in Opti-MEM and transfected per 16,000 cells.

Viral production – recombinant adeno-associated virus 1/2-HA-Ast-3-mCherry

HEK293 viral cells (HEK293FT) were maintained at similar conditions to HEK293T cells and in complete DMEM which was supplemented with an additional 2% 100x non-essential amino acids and 2% 100x sodium pyruvate (Invitrogen). HEK293FT cells at less than 30 passages, were seeded into ten 20 cm^2 culture dishes (Nalgene Nunc, ThermoFisher) at $1x10^7$ cells per dish. On the next day, they were transfected using a PEI transfection protocol (Huang et al., 2013), with 50 μg of the pAM-HA-Ast-3-mCherry, and helper plasmids pDPI and pDPII (Grimm et al., 2003) in equimolar amounts at a ratio of 4.5 pDPI+pDPII: 1 pAM-HA-Ast-3-mCherry. Five to 6 h after transfection, the media was replaced, and cells were placed in an incubator for 72 h at 37°C in 5% CO_2. Transfection efficiency was visualized using red fluorescence from mCherry. Cells were dissociated from cell culture flasks with trypsin/EDTA, collected in their media from 20 cm^2 culture dishes and spun at 2100 rpm for 5 min to pellet cells. The cell pellet containing the viral particles was resuspended in 1 mL of lysis buffer (150mM NaCl, 50mM Tris-HCl, pH 8.5) per 20 cm plate and subjected to a series of 4 freeze-thaw cycles by alternating the cell mixture between a water bath (37°C) and liquid nitrogen (−196°C). The mixture was vortexed briefly between each freeze-thaw cycle. Benzonase endonuclease (Sigma-Aldrich, Australia) was added to the lysate, to a final concentration of 50U/mL, and the solution vortexed and incubated for 1 h at 37°C. Cell debris was pelleted through centrifugation (20 min at 4050 rpm) and the supernatant filtered through a 13 mm diameter 45 μm Acrodisc filter, to produce a crude virus lysate. The viral transgene expression was assessed by transducing HEK293FT cells and examining fluorescence after 3 days incubation.

Recombinant adeno-associated virus purification and viral titration

The rAAV particles were purified and concentrated using an iodixanol density centrifugation (Zolotukhin et al., 1999). Virus supernatant was added to a density gradient made up of 15%, 25%, 40%, and 54% iodixanol from a 60% (w/v) iodixanol solution, Optiprep (Sigma-Aldrich). Phenol red (100 μL) was added to the 25% and 54% solutions to enable distinction between layers. Quickseal tubes were heat sealed and spun in an Himac CP-MX Series preparative ultracentrifuge (Hitachi Science & Technology, Germany) at 65,000 rpm for 80 min at 18°C. As the density of an rAAV is 1.24 g/mL, the band containing the viral particle falls at the 40% interface and was isolated. These layers from each flask were pooled, put into an ultra-centrifugal filter device (1,000,000 MW; Millipore, Australia), dialysed with 0.1 M PBS, and spun at 4000 rpm for 40 min, filling the centricon filter device with ~15 mL 0.1 M PBS and filtered products after each spin. Once the virus was no longer displaying a pink hue, from the phenol red, a final centrifugation was performed for 30 min without PBS giving a final volume of 200-250 μL. This purified virus, denoted rAAV1/2-HA-Ast-3-mCherry, was collected and stored at −80°C in 5 μL aliquots.

To qualitatively assess viral titer, HEK293FT cells were plated with complete DMEM at 10,000 cells per well in a 24-well plate (Nalgene Nunc, ThermoFisher Scientific). The next day the cells were transduced with a serial dilution of purified rAAV1/2-HA-Ast-3-mCherry at neat; 1:10; 1:100; or 1:1000 dilutions. Each viral dilution was made up in 1 mL of media that was added to the cells. Cells were incubated for 72 h at 37°C with 5% CO_2 in a water jacket incubator and mCherry fluorescence examined after 5 days, using an upright fluorescent microscope (Olympus IX70, Life Sciences, Australia). If fluorescence was absent or minimal, cell media was changed, and cells were left for a further 48 h.

To determine the number of genomic copies of virus per unit volume, the rAAV1/2-HA-Ast-3-mCherry was lysed in dilution buffer (1:4 ratio virus:buffer) at 56°C for 30 min, and a 1:100 and 1:1000 dilution was used in a qPCR reaction. A standard curve of pAM-HA-Ast-3-mCherry was produced, using molecular weight of the plasmid to calculate 10^{10} plasmid copies per 5 μL and then generate standards estimated to contain 10^9, 10^8, 10^7, 10^6, 10^5, 10^4, 10^3 copies per 5 μL in dH_2O. The qPCR reactions were conducted in triplicate in 25 μL/well of a MicroAmp® 96-well plate (Nalgene Nunc, ThermoFisher Scientific). The reaction contained 12.5 μL of SYBR® Green Mastermix, 5 μL of diluted rAAV1/2-HA-Ast-3-mCherry or pAM-HA-Ast-3-mCherry standard, 1 μL of both Woodchuck Posttranscriptional Regulatory Element (WPRE) forward and reverse primers at 10 μM, made up to 25 μL with dH_2O. Distilled H_20 was used as a negative control. The qPCR amplification was conducted on a Vii7 real-time PCR system (ThermoFisher Scientific) with the conditions: 2 min at 50°C, 10 min at 95°C (pre-denaturation), 40 cycles of denaturation at 95°C for 15 s and annealing/extension at 60°C for 1 min, with a dissociation step included at the end, 95°C for 15 s, 60°C for 1 min, 95°C for 15 s and finally 60°C for 15 s. The threshold cycle (C_T) of each standard and rAAV1/2-HA-Ast-3-mCherry dilution was analyzed using linear regression, and the rAAV1/2-HA-Ast-3-mCherry genomic copies per mL, calculated from the average of the 1:100 and 1:1000 dilutions, was $5.08x10^{11}$ genome copies/mL.

Viral production - Lentivirus

The generation of lentiviral (Lv) vectors expressing the AstR-p2A-GFP (Lv-PRSx8-AstR), or GFP alone (Lv-PRSx8-GFP), under the control of a multimeric Phox2 binding site promoter (PRSx8), has been described previously (Chen et al., 2010; Marina et al., 2011). HEK293T cells were plated out in 2x10 cm^2 plates one day prior to transfection at $4x10^6$ cells per plate and a confluency of 40%–60% on the day of transfection. They were transfected with 3mL of Opti-MEM, containing Lipofectamine2000; 8 μg of pTYF-PRSx8-AstR-p2A-GFP (Figure S1D; AddGene #159632) or pTYF-PRSx8-GFP (Figure S1E); 5.2 μg of pMDL; 2 μg of pRSV-Rev; and 2.8 μg of pCMV-VSV-G (Chang et al., 1999). The DNA/Lipofectamine2000 mixture was added drop wise to each dish and incubated overnight in 37°C/5% CO_2 incubator. Media was collected after 48-60 h incubation into a 50 mL conical centrifuge tube and spun for 5 min at 2000 rpm to pellet cellular debris. Medium containing virus was then filtered through a 45 μM filter unit and loaded into 38.5 mL ultracentrifuge tubes (Beckman polyallomer, ultraclear tubes) containing a 220 μL cushion of 60% iodixanol solution and spun at 20,000 rpm for 2.5 h at 4°C in a Beckman SW32Ti swinging bucket rotor. Media-iodixanol solution was collected from the bottom of each tube (~750 μL), mixed, pooled and transferred to a 50 mL tube and made up to 25 mL with PBS. The viral solution was loaded into 5 mL ultracentrifuge tubes and spun at 7000 rpm at 4°C for 24 h in a Beckman SW-50.1 swinging bucket rotor. Subsequently, the supernatant was discarded, and viral pellet was resuspended in 15 μL of PBS for 24 h at 4°C. The virus was mixed by gently pipetting and then aliquoted and stored at −80°C. The titer, determined by qPCR, was 3.76×10^9 infectious units per mL for Lv-PRSx8-AstR and 6.9×10^9 infectious units per mL for Lv-PRSx8-GFP.

Production of CHO-AstR cells

To test bioactivity of Ast peptides, including that produced by rAAV1/2-HA-Ast-3-mCherry transduction, we generated a cell line stably expressing the AstR and GFP. Initially, a plasmid vector, containing a chicken beta-actin promoter driving the expression of AstR and GFP, was cloned to ensure robust gene expression and production of recombinant lentivirus in HEK293T cells. The AstR-IRES-GFP coding region (2.7 kb) was excised from the pAAV-hSyn-AstR-IRES-GFP construct (Tan et al., 2006) with Sal1 and ligated into the pTYF-CBA viral vector which was linearized with XhoI to produce pTYF-CBA-AstR-IRES-GFP (Figure S1C). Following plasmid construction, HEK293T cells were plated out at $4x10^6$ cells per 10 cm^2 plate, one day prior to transfection, and the host CHO-KI cells were plated out at $2x10^5$ cells per 10 cm^2 plate, to be subconfluent within two days. HEK293T cells were transfected with 3 mL of Opti-MEM containing Lipofectamine2000 (50 μL), plasmid construct (8 μg of pTYF-CBA-AstR-IRES- GFP) and packaging plasmids (5.2 μg of pMDL; 2 μg of pRSV-Rev; and 2.8 μg of pCMV-VSV-G). Following overnight incubation at 37°C in 5% CO_2, media from transfected HEK293T cells was collected, filtered through a 0.45 μm filter and supplemented with polybrene. Transfected HEK293T cells were replenished with 10 mL of fresh DMEM complete media and filtered infectious media was added onto subconfluent CHO-K1 cells. This process was repeated twice per day (morning and afternoon) for 2 consecutive days, with cells allowed to recover subsequently for three days. CHO-K1 cells were then trypsinised from cell culture plates and harvested into T175 cm^2 flasks for fluorescence-activated cell sorting (FACS) to sort high, medium, and low expressing GFP cells which denoted AstR expression. Fluorescent protein expression was analyzed on a FACSCalibur (BD Biosciences, USA) using argon-ion laser excitation (488 nm) and detected using the FL1 parameter (emission filter: 530 ± 15 nm). Data acquisition was carried out by analyzing 10,000 events/sample using Cell Quest software version 5.1 (BD Biosciences, Australia). CHO-K1 cells expressing high levels of GFP (CHO-AstR stable) were sorted, maintained in T175 cm^2 and used for cell-based assays.

Measurement of cAMP

To test the bioactivity of synthetic Ast-3, HA-Ast-3 or potential HA-Ast-3 transgene produced by pAM-HA-Ast-3-mCherry, a pCRE reporter gene assay (Bathgate et al., 2006), assessing receptor cAMP signaling, was performed in CHO-AstR cells. We measured the inhibition of cAMP induced by increasing concentrations of synthetic Ast-3 or HA-Ast-3 peptide (0.001 – 100 nM). To measure secreted peptide following transfection with pAM-HA-Ast-3-mCherry, HEK293T cells were plated at $1x10^6$ cells per well into 6-well plates pre-coated with 0.1 mg/mL poly-D-lysine. Prior to addition of transfection mixture, the cells were supplemented with fresh complete DMEM media. The cells were transiently transfected by exposure to 5 μg of pAM-HA-Ast-3-mCherry, or pcDNA3.1 (+) as a control, and Lipofectamine2000, made up in Opti-MEM. Plates were incubated at 37°C, 5% CO_2 for 48 h. The media was collected and stored at −20°C before testing in the cAMP assay described above. Increasing dilutions of the conditioned media, in complete DMEM (1:1000, 1:100, 1:50, 1:25, 1:10 and 1:5) were measured.

CHO-AstR cells were resuspended in media and plated out into 96-well plates (Eppendorf cell culture plates) at 8,000 cells/well. Cells were transfected with a pCRE-β-galactosidase (β-gal) reporter gene to indirectly report on cellular cAMP activity. As the AstR is a $G_{i/o}$ coupled receptor the cells were first stimulated with 500 nM forskolin to increase cAMP activity. Synthetic peptides or conditioned media were incubated with CHO-AstR cells, transfected with pCRE-β-gal reporter gene, for 6 h at 37°C in a 5% CO_2 water jacket incubator. After 6 h, the media was removed, and the cells were subjected to a colorimetric assay to determine β-gal activity as a measure of cAMP activity. The colorimetric assay involved incubating the cells with 25 μL Assay buffer 1 (10 mM sodium phosphate buffer, 0.2 mM $MgSO_4$, 0.01 mM $MnCl_2$, pH 8.0) 100 μL of Assay buffer 2 (100 mM Na_2HPO_4, 2 mM $MgSO_4$, 0.1 mM $MnCl_2$, 0.5% Triton X-100, 40 mM β-mercaptoethanol, pH 8.0) and 25 μL of enzyme substrate solution (1 mg/mL chlorophenol red-β-D-galactopyranoside, 100 mM Na_2HPO_4, 2 mM $MgSO_4$, 0.1 mM $MnCl_2$, pH 8.0). Following incubation at room temperature (RT) on an orbital shaker, for 10 min – 1 h until absorbance readings reached values indicating maximum inhibition $\leq$ 0.3 or no inhibition $\geq$ 1.0 of forskolin-induced cAMP activity, absorbance readings were conducted to determine cAMP accumulation and receptor

inactivation. The absorbance of each well was determined at 570 nm using a Benchmark-Plus Microplate Spectrophotometer (Bio-Rad Instruments, Australia). These experiments were repeated at least three times, with triplicate determinations within each assay.

Synthetic peptides

Synthetic allatostatin-3 (Ast-3; SRPYSFGL, M.W. 926.04) and N terminus hemagglutinin tagged Ast-3 (HA-Ast-3, YPYDVPDYA-Ast, M.W. 2010.19) were purchased from GL Biochem Ltd (Shanghai, China; HPLC purified, > 90% purity). Both of the peptides underwent in-house validation and purity testing by reverse phase HPLC and matrix-assisted laser desorption/ionisation – time of flight (MALDI-TOF) mass spectrometry analysis.

In vivo validation - General surgical procedures

All surgeries were performed under sterile conditions with the surgical plane determined by loss of pedal withdrawal and corneal reflexes. Analgesia (meloxicam, 1 mg/kg, s.c.; Metacam, Boehringer Ingelheim, Australia) was provided. For all surgical procedures, anesthesia was induced by inhalation of 4%–5% isoflurane (Abbott Laboratories, United States) in air in a sealed container. Surgical anesthesia was provided by intramuscular (i.m.) injection of a mixture of ketamine (60 mg/kg; Lyppard, Australia) and medetomidine (250 μg/kg; Pfizer Animal Health, Australia), with depth of anesthesia assessed by loss of the pedal withdrawal and corneal reflexes. The surgical field was shaved and disinfected with 80% ethanol, chlorhexidine and betadine antiseptic solution. A wetting gel (Polyvisc) was applied to the eyes to prevent drying. After completion of the surgery, rats received an injection of warmed Hartmann's solution (1 mL, i.p.; Baxter Healthcare, Australia) and anesthesia was reversed with atipamazole (1 mg/kg, i.m.; Pfizer). Rats were placed on a heat mat for recovery, prior to being returned to their standard cage, single housed for 24 h post-surgery and then re-combined with littermates. Rats were monitored twice daily for 4 days after surgery and once daily thereafter assessing coat condition, bodyweight, general responsiveness and activity, and wound healing or any signs of infection.

Injections into the nodose ganglion

Once a deep surgical level of anesthesia was obtained, rats were placed supine on a heating blanket and a midline longitudinal incision made between the attachment of the digastric muscle anteriorly and the clavicle posteriorly. Using blunt dissection, the platysma muscle was moved to expose the sternohyoid and omohyoid muscles. These two muscles were separated and retracted to expose the common carotid artery and its bifurcation. The vagus nerve was identified beside the common carotid artery. The superior laryngeal nerve was identified and followed to its connection with the vagus nerve. This was defined as the posterior border of the nodose ganglion (NDG). The digastric muscle was retracted laterally to expose the NDG. A 30 g needle was used to gently scrape along the capsule surrounding the NDG to enable a glass pipette to penetrate. Five μL of the virus was mixed with ~200 nL of 1% Fast Green dye (Sigma-Aldrich), to aid visual observation of virus injection, and loaded into an injection pipette (1 mm borosilicate glass capillary tubing (World Precision Instruments, USA) pulled in a vertical pipette puller (Narishige Scientific Instrument Lab, Japan) with the tip broken to provide 30 μm outside tip diameter) by back-filling. The virus was injected with a picospritzer (World Precision Instruments) connected to the pipette glass by 1.0 mm polyethylene (PE) tubing to enable injections to be made using pulses of pressurized nitrogen gas. The pressure was adjusted to allow the virus to be delivered in multiple small volumes (1-5 nL per pulse) with final volumes delivered at a rate of ~50 nL/min. Upon completion of the injection the incision was closed with Safil (4/0) absorbable suture material and the rats were allowed to recover.

Injections into the nucleus of the solitary tract

Once anesthetised and prepared for surgery, rats were placed on a heating mat (37°C) in a stereotaxic frame (RWD Life Science, ShenZhen, China). The head was ventroflexed and incisors secured over the bite bar at −15 mm. A dorsal midline incision was made between the first cervical vertebra and the occipital bone and the muscles separated to expose atlanto-occipital membrane. A small section of the occipital bone, at its connection with the atlanto-occipital membrane, was removed with a dental drill enabling access to the underlying brain structures. The dura was cut in the midline and cleared laterally to expose the dorsal surface of the brainstem. The pipette was connected to a picospritzer as described above. To cover larger areas of the NTS, multiple injections of 50 nL were made into different sites. Following each injection, the injector was left in place for 3 min, moved dorsal by 0.1 mm and left for a further 2 min and then moved to the next coordinate. Upon completion of the injections, the incision was closed with Safil (4/0) absorbable sutures and the rat recovered.

Protocols

Expression of rAAV1/2-HA-Ast-3-mCherry in the brainstem

In SD rats (n = 4), rAAV1/2-HA-Ast-3-mCherry was injected into the region of the caudal NTS (cNTS), underlying dorsal motor nucleus of vagus and hypoglossal nucleus at the following coordinates (in mm): 0.2 caudal to obex; 0.1 lateral to midline and 0.4 and 0.6 from the surface of the brainstem.

Expression of rAAV1/2-HA-Ast-3-mCherry in the nodose ganglion

In SD rats (n = 8), rAAV1/2-HA-Ast-3-mCherry was injected into the NDG to test expression and optimize the injection protocol. We tested the efficacy of expression following: a single injection of 750 nL of virus; a single injection of 500 nL of virus; 5 injections of 100 nL each into different parts of the NDG (total volume of 500 nL); 5 injections of 150 nL each into different parts of the NDG (total volume

of 750 nL). *Post-mortem* analysis of both the NDG and afferent labeling in the NTS revealed that best transduction occurred with a single 750 nL injection and this protocol was used for all subsequent experiments.

Patch clamp recordings of transduced NTS neurons in slices

For patch clamp studies, to increase the number of cells available for recordings, 50 nL Lv injections were made into the cNTS at the following 18 sites for a total of 900 nL per SD rat (Table 1). Injections were made 0.4 and 0.2 mm from the dorsal brain surface at the following coordinates, relative to obex. For each injection tract, the ventral injection was made first.

For examining the effect of synthetic Ast-3 and HA-Ast-3 on NTS neurons, brainstem slices were prepared from SD rats 62 ± 15 days after the NTS injection (n = 13; 610 ± 29 g on recording day). For synaptic studies, rAAV1/2-HA-Ast-3-mCherry was injected into the NDG using the optimized injection protocol, in preparation for patch clamp studies to examine Ast release with high frequency stimulation. Two weeks later Lv-PRSx8-AstR or Lv-PRSx8-GFP were injected into the cNTS as described above. Brainstem slices were prepared from SD rats 40 ± 1 days after the NTS injection (n = 8; 498 ± 13 g on recording day). Rats were deeply anaesthetised with 5% isoflurane and the medulla removed, blocked and rapidly cooled in artificial cerebrospinal fluid (aCSF, 2°C, containing (in mM): NaCl, 125; KCl, 3; KH_2PO_4, 1.2; $MgSO_4$, 1.2; $NaHCO_3$, 25; dextrose, 10; $CaCl_2$, 2; (300 mOsmol)). Both coronal and horizontal 250 μm slices of the dorsal medulla, that contained both the solitary tract (ST) and the NTS, were cut on a vibratome (VT1200s; Leica Microsystems). The slices were continuously perfused in aCSF solution, bubbled with 95% O_2, 5% CO_2, at 32°C.

Recording pipettes (2.6 – 6.5 MΩ) were filled with an internal solution containing (in mM) NaCl, 6; NaOH, 4; K, 130 (OH and gluconate); EGTA, 11; $CaCl_2$, 1; HEPES, 10; $MgCl_2$, 1; and 0.1% biocytin (pH 7.3, 290 mOsmol, E_{Cl} −68.8 mV). Pipettes were visually guided to GFP-expressing NTS neurons using a fixed stage microscope (Zeiss Examiner) and camera (*Rolera EM-C2,* Q-Imaging, Canada). Whole-cell recordings were made in either voltage clamp (holding voltage (V_H) −60 mV or −40 mV) or current clamp mode (MultiClamp 700B and pClamp 10.3, Molecular Devices, CA). Signals were sampled at 20 kHz and filtered at 10 kHz. Liquid junction potentials were not corrected (−6.2 mV at 32°C) until post hoc analysis. Ast (5 nM) and HA-Ast (100 nM) was superfused onto the slice in aCSF at 2.5 mL/min.

For synaptic studies, all neurons were first classified as receiving vagal afferent input, or not, in voltage clamp mode. Primary afferent axons within the ST were activated by electric stimulation using a concentric bipolar electrode (200 μm outer diameter; FHC, USA) that was placed on the visible ST at a distance of 2-3 mm from recorded neurons. Trains of 5 shocks (100 μs) at 50 Hz, where intensity was varied (0.03-0.5 mA), evoked ST-EPSCs. NTS neurons were classed as a second order neuron, directly receiving primary afferent input, if ST-EPSCs exhibited a synaptic jitter (standard deviation of EPSC latency) of less than 200 μs and exhibited frequency-dependent depression. Otherwise neurons were classified as higher order. High frequency stimulation of the ST (ST-HFS) was carried out at 50 Hz (100 μs shocks) for 2 or 30 s in current clamp mode (I = 0 pA). Likewise input-frequency curves were recorded in current clamp at I = 0 pA, prior to and after ST-HSF in aCSF; prior to and after ST-HSF in ionotropic receptor blockade (NBQX 20 μM, AP-5 100 μM and Gabazine (SR-95531) 3 μM; Tocris, USA) confirmed by ST-EPSC block and after TTX (1 μM; Tocris, USA) to confirm action potential block.

Expression of rAAV1/2-HA-Ast-3-mCherry in nodose ganglion and Lv-PRSx8-AstR or Lv-PRSx8-GFP in NTS of blood pressure telemetered SHR

Male SHR (n = 18; ∼250 g) were purchased in 3 separate cohorts of 6, 2, and 10 animals. Within each cohort, animals were assigned at the start of the protocol to SHR Experimental – those that would eventually receive injections of Lv-PRSx8-AstR into the NTS (n = 9) – and SHR Control – those that would receive injections of Lv-PRSx8-GFP into the NTS (n = 9). One rat was excluded from the SHR Control cohort as it was delivered at an older age with a higher bodyweight and BP, leaving a cohort of n = 8. In all other regards the animals were treated identically.

In the first surgery, rAAV1/2-HA-Ast-3-mCherry was microinjected into the NDG bilaterally. The SHR were allowed to recover in their home cage for 2 weeks, with daily measurement of bodyweight between 8:00 and 10:00.

In the second surgery, 14 ± 4 days after the NDG injections, BP telemeters were implanted into the abdominal aorta of SHR anesthetized as described above. Following surgery, the rats were returned to their home cages for recovery for 2 weeks before commencement of control BP recordings. Telemetry devices for recording blood pressure (BP; TA11PA-C40 telemeters; Data sciences International, USA) were implanted following the manufacturer's protocol. Briefly, the abdominal cavity was opened in the midline and the pressure sensing catheter inserted into the abdominal aorta distal to the renal arteries. Vetbond was applied to seal the vascular opening and ensure attachment to the abdominal aorta. The transmitter probe was placed in the abdominal cavity and sutured to the abdominal muscle layer. After 2 weeks, 3 baseline BP recordings were taken for each rat on separate days.

In the third surgery, 3 weeks after the telemeter implant, Lv injections were made into the cNTS. In order to keep viral injection volume at any one site to 50 nL, and to ensure coverage of the NTS with a Lv that doesn't spread through the brain as efficiently as an rAAV, we injected at the following 7 sites for a total of 350 nL per rat. Injections were made 0.4 from the dorsal brain surface at the following coordinates, relative to obex (Table 2).

Following injections, the rat's bodyweight was measured daily. As only four telemetry plates were available for recording BP at any time, rats in cohorts 1 and 3 were assigned to separate subgroups (n = 3 per subgroup). A 2.5 h recording of BP was made from each subgroup every day in the period between 8:00 and 15:00, being the quiet period 2 h after lights on and at least 3 h before lights off. Measurement of circadian variation of BP indicate that it is stable during this period (Osborn and Hornfeldt, 1998). The timing of the

2 h recording period during this time was randomized between sub-groups on different days. Each subgroup was also measured for the remainder of the day:night cycle every 3rd day to assess BP across the circadian period (Figure S2).

Commonly in BP telemeter studies, investigators obtain average readings of BP over defined periods – e.g., 10 min averages. This approach was applied to the first SH rat cohort (n = 3 per group). However, when observing real-time recordings, we noticed spurious, movement related fluctuations in BP that were clearly non-physiological - BP readings in excess of 300 mmHg. These were relatively random, occurred to different degrees among animals during the same recording period and resulted in increased signal variability that did not reflect a biological signal. As a result, for further recordings we sampled waveform BP data at 2000 Hz, using an analog-to-digital data acquisition card (PCI-8024E; National Instruments, Australia), imported the signal into Spike2 (Cambridge Electronic Design, UK) and analyzed the data offline. All points in excess of 300 mmHg were removed and replaced with the average of the preceding 1 s of data. We compared the resultant data based on this method with the automatic average data and determined that such interference results in random shifts, both up and down, in average BP readings that can be of a magnitude of 10-15 mmHg over a 2 h recording period. As a result, the data included in the manuscript is from a 2h recording period, excluding the 30 min immediately after handling to turn on the BP telemeter, and is only based upon those SH rats in the second and third cohort which had noise readings removed (SHR Experimental (n = 6); SHR Control (n = 5)). The measurements were normalized to the control period for each animal and then presented as mean ± 95% confidence intervals for the groups, with each individual animal also shown. For completeness of the dataset, all raw BP data from all SH rats (SHR Experimental (n = 9); SHR Control (n = 8)) are shown (Figure S2B). Analysis of the data which included all animals shows the same overall response, with just an alteration in the number of days that were significantly different between groups.

Systolic, mean and diastolic BP and heart rate (HR) were derived from the pulsatile arterial BP trace. The systolic BP was used as a surrogate measure of the cardiac R-wave and the time between successive pressure maxima as the interbeat interval (IBI). The standard deviation of BP and IBI were derived and plotted for each animal. The baroreceptor sensitivity (BRS) was determined with the sequence method (Kuusela, 2013), and defined as the relationship between a change in the IBI following a unitary change in BP (ms/mmHg). Individual points for systolic BP and IBI were examined in 10-20 min sections during quiet, inactive periods between 11:00 h and 13:00 h. The data were analyzed using a custom-made MATLAB script that identified periods in which systolic BP and IBI rise or fall monotonically in the same direction for at least three beats, exceeding or meeting a defined threshold of a change of 0.5 mmHg and 1 ms respectively (Figure S3A). The IBI series was advanced by one beat to adjust for the delay between BP and corresponding changes in IBI. A minimum correlation co-efficient (> 0.8) between systolic BP and IBI had to be achieved for the script to consider an actual BRS sequence. Finally, the BRS of each sequence was calculated by the slope of the regression line of systolic BP versus IBI, and the BRS of an animal was the average slope calculated from all the sequences found. Mean slopes of BRS for sequences where systolic BP and IBI increased (called UP-UP, with increased IBI representing a decreased in HR; Figure 4G) were assessed separately from those in which systolic BP and IBI decreased (DOWN-DOWN; Figure S3B). The number of UP-UP and DOWN-DOWN sequences were quantified. Values for all parameters are expressed as individual animals and mean ± 95% confidence intervals for the groups.

Expression of rAAV1/2-HA-Ast-3-mCherry in nodose ganglion and Lv-PRSx8-AstR in NTS of SD rats

Twenty male SD rats were assigned at the start of the protocol to SD. Experimental – those that would eventually receive injections of Lv-PRSx8-AstR into the NTS (n = 10), and SD. Control – those that would receive injections of Lv-PRSx8-GFP into the NTS (n = 10).

In the first surgery, rAAV1/2-HA-Ast-3-mCherry was microinjected into the NDG bilaterally. The SD rats were allowed to recover in their home cage for 2 weeks, with daily measurement of bodyweight. After 2 weeks, Lv injections were made into the cNTS at a total of 7 different sites, with 50 nL at each site and a total volume of 350 nL per rat, as described for the SHR above (Table 2). The rats were returned to home cages, re-housed with littermates and weighed daily for the next 31 days.

Two additional control SD groups were also generated with microinjections into the cNTS, as described above. The first extra control cohort received just Lv-PRSx8-AstR (n = 10) or just Lv-PRSx8-GFP in the cNTS (n = 10). The second extra control cohort (n = 10) received a unilateral injection of rAAV1/2-HA-Ast-3-mCherry in the NDG, followed 2 weeks later by injection of Lv-PRSx8-AstR in the cNTS, as described previously (Table 2). Following completion of the surgeries the rats were re-housed and bodyweight measured for 14 days.

Bodyweight data are shown in the text as change in bodyweight from the pre-surgery values as growth rates varied naturally between rats and there were minor differences in timing between sections. For completeness, actual bodyweights are shown for all animals (Figure S4).

Tissue perfusion

At the completion of each protocol, the rats were deeply anesthetized, by inhalation of 4%–5% isoflurane in a sealed container, followed by injection of a mixture of ketamine (60 mg/kg) and medetomidine (250 μg/kg) i.m., and killed by intracardiac perfusion using a peristaltic pump (Cole-Parmer Masterflex L/S Drive System, USA) delivering 0.1 M phosphate-buffered saline (PBS), followed by 4% paraformaldehyde in 0.1 M PBS at a rate of ~30 mL/min. The brains were removed and post-fixed in 4% paraformaldehyde in 0.1 M PBS for 6 h at RT, followed by immersion in 20% sucrose at 4°C until processing for immunohistochemistry. The thorax and head were post-fixed in 4% paraformaldehyde in 0.1 M PBS overnight and then washed several times with 0.1M PBS over the following

24 h. The NDG were dissected out along with the distal vagal trunk and the superior laryngeal nerve, to its entry to the posterior lacerated foramen. It was then immersed in 20% sucrose at 4°C until processing.

Immunohistochemistry

The details of all antibodies used in the study, including dilutions used in the NDG or brainstem, are provided in the Key Resources Table.

Nodose ganglia

The expression of mCherry and neurophysin I was examined in the NDG. The ganglia were embedded in optimal cutting temperature compound and frozen on a cryostat chuck at −20°C. Sections (20 μm thickness) were cut in the cryostat (HM525, Microm, Germany), mounted directly onto gelatin-coated slides, and stored at −20°C. Prior to immunostaining, a hydrophobic barrier was traced around the sections using an ImmEdge Hydrophobic Barrier PAP Pen (Vector Labs). The slides were washed with immunobuffer (IB) (1xTPBS (10 mM Tris-HCl, 154 mM NaCl, 1.24 mM merthiolate in 0.1 M sodium phosphate buffer, pH 7.4) containing 0.3% (v/v) Triton X-100; 3 × 10 min) before incubation at RT in IB containing 10% normal horse serum (NHS, Invitrogen; 30 min). The solution was then replaced with IB containing 10% NHS and primary antibody for 24 h in a humidified sealed container at 4°C. The slides were then washed with 1x TPBS (3 × 10 min), incubated with secondary antibody in IB containing 10% NHS for 1h at RT, and then washed with 1xTPBS (3 × 10 min). The PAP pen barrier was removed, and the slides were coverslipped using Cytoseal60 (ProSciTech, Australia). Slides were stored in the dark prior to imaging.

Brainstem sections

The rat brainstem, including the NTS, was frozen at −20°C, and coronal sections (40 μm thickness) cut using a cryostat. The sections were placed directly into cryoprotectant (0.88 M sucrose, 0.25 mM polyvinyl-pyrrolidone, 4.35 M ethylene glycol, 50 mM sodium phosphate buffer, pH 7.2) in a 24-well plate and stored at −20°C until processing for immunohistochemistry. To obtain representative samples of the NTS, a 1:6 series of sections was processed for each combination of antibodies. The sections were removed from storage buffer and processed free-floating for immunohistochemistry using the same procedures as described for NDG sections, with the following alterations. Sections were incubated in primary antibody solution for 3 days and secondary antibody solution for 4 h, on an orbital shaker, at RT. The container was covered with aluminum foil during incubations.

Microscopy

Epi-fluorescent images were obtained using a Nikon microscope (Nikon, Australia) with a MR3 digital camera. Confocal images of immunofluorescence in the rat brain and NDG were acquired using a Zeiss 780 axio confocal microscope (Zeiss, Australia). A consistent pinhole setting of 1.0 μm was used. Some higher power images were acquired with a 20x or 63x objective and as an image stack (4x4), with 0.8 μm or 0.26 μm z axis interval. Between 11 and 15 images were collected for stacks at 20x magnification and 27-35 for stacks at 63x magnification. Maximum intensity projections of image stacks were produced using ZEN microscopy software (Black edition SP1, version 8.1, 2012). Excitation and emission wavelengths were: Cy-3: 550 nm and 570 nm; Alexa 488: 495 nm and 519 nm and Cy-5: 650 nm and 665 nm. Images, along with overlays and tiling, were created using Zen Black software. For publication images, with scale bars embedded, were exported as tiff files into Photoshop (Adobe CC 2020) where the contrast for the entire section was optimized and the color for each label coordinated. The image was then imported into Illustrator (Adobe CC 2020), magnified and cropped to show relevant features.

Mapping of transduced neurons in the nucleus of the solitary tract

The distribution of transduced NTS neurons, following microinjections of Lv-PRSx8-AstR (which also expresses GFP) or Lv-PRSx8-GFP, were mapped onto schematic maps of the NTS derived from The Rat Brain in Stereotaxic Coordinates (Paxinos and Watson, 2006) using Inkscape software (version 0.92.4, 2019). The distribution of ChAT and TH immunoreactive neurons was used to accurately map the anatomical positions of transduced neurons. The distribution of mCherry-expressing vagal afferent axons, arising from transduced NDG cell bodies, was also mapped onto the NTS schematics. Mapped NTS schematics of each rat, from each experimental cohort, were combined to form heatmaps. The opacity of each NTS schematic from each rat was reduced evenly across the group, this enabled the opacity to reach 100% in specific areas on the NTS schematic when a similar transduction profile was observed in all rats. The two maps were overlayed. *Post hoc* immunohistochemical analysis, to verify expression of GFP labeling in the NTS and overlapping mCherry labeling in the vicinity of the GFP cells, was an inclusion criterion for the study. This was observed in all animals and so all were included in the final data presented.

QUANTIFICATION AND STATISTICAL ANALYSIS

All statistical analysis was performed using GraphPad Prism 8.1 software (Graphpad Inc., USA). The cAMP measurements were normalized against the forskolin response (500 nM) and plotted as mean ± standard error of the mean (SEM). For electrophysiological analysis; membrane potential measurements were averaged over 1 min immediately prior to (baseline) ST-HFS or peptide superfusion and over a 1 min period of maximum hyperpolarisation thereafter (in both non- and responding neurons). Paired t tests were run

in each condition comparing the post membrane potential to baseline. For input frequency curve comparisons (step protocols) a two-way ANOVA was used. Synaptic jitter was defined as the standard deviation of the latency ST-EPSCs (shock 1 of 5) over 10-20 trials (electric shocks). Frequency-dependent depression was defined as paired pulse ratios less than 1.0 as calculated from ST-EPSC$_{2\text{-}5}$ as a ratio of ST-EPSC$_1$. Data are presented as mean ± SEM. For *in vivo* studies all data are presented as mean ± 95% confidence intervals (CI). Differences in measured parameters between the groups prior to surgery were analyzed using an unpaired Student's t test. Cardiovascular measurements (systolic BP, diastolic BP, mean BP and HR), baroreceptor reflex sensitivity, quantification of the number of sequences detected during rises and falls in systolic BP and bodyweight data following each surgery were analyzed by a two-way repeated-measures analysis of variance, with a Bonferroni post-test. Values were considered significant if $p < 0.05$.